J. Fluid Mech. (1990), *vol.* 211, *pp.* 557–593
Printed in Great Britain

The complete second-order diffraction solution for an axisymmetric body Part 2. Bichromatic incident waves and body motions

By MOO-HYUN KIM AND DICK K. P. YUE
Department of Ocean Engineering, Massachusetts Institute of Technology, Cambridge, MA 02139, USA

(Received 30 May 1989)

In Part 1 (Kim & Yue 1989), we considered the second-order diffraction of a plane monochromatic incident wave by an axisymmetric body. A ring-source integral equation method in conjunction with a novel analytic free-surface integration in the entire local-wave-free domain was developed. To generalize the second-order theory to irregular waves, say described by a continuous spectrum, we consider in this paper the general second-order wave–body interactions in the presence of bichromatic incident waves and the resulting sum- and difference-frequency problems. For completeness, we also include the radiation problem and second-order motions of freely floating or elastically moored bodies. As in Part 1, the second-order sum- and difference-frequency potentials are obtained explicitly, revealing a number of interesting local behaviours of the second-order pressure. For illustration, the quadratic transfer functions (QTF's) for the sum- and difference-frequency wave excitation and body response obtained from the present complete theory are compared to those of existing approximation methods for a number of simple geometries. It is found that contributions from the second-order potentials, typically neglected, can dominate the total load in many cases.

1. Introduction

Many compliant offshore structures are designed to have their natural frequencies of oscillations above and/or below that at which significant ocean wave energy is present. This avoids possible large responses at wave frequencies due to linear excitations. When second-order effects are included in the presence of irregular waves, there are in general excitations at the sums and differences of the component frequencies. Although the magnitudes of these nonlinear effects are in general second-order, they may be of primary concern when such excitations are near the natural periods of body motions and when the corresponding damping forces are small. Typical examples are the low-frequency horizontal-plane motions of moored ships and vertical-plane motions of small-waterplane-area vessels for difference-frequency excitations; and the high-frequency vertical-plane oscillations of tautly moored bodies such as tension-leg platforms, and 'springing' vibrations of ship hulls for the sum-frequency forces. In these cases, the linearized theory often does not provide even a first approximation for predicting the loads and motions.

For a single regular incident wave, the complete second-order diffraction solution for vertically axisymmetric bodies was presented in Part 1 (Kim & Yue 1989;

hereinafter referred to as KY-I). The second-order (double-frequency) potential and associated local quantities were obtained explicitly using a boundary-integral formulation involving general order free-surface ring-source Green functions. A powerful treatment of the requisite free-surface integral involving analytic integration of local-wave-free modes was developed resulting in rapid exponential convergence of the integral with truncation radius. The efficacy and accuracy of the method was established through systematic convergence tests and comparisons to available analytic and semi-analytic results.

In this paper, we consider the generalization of the second-order theory to Gaussian irregular incident waves, say given by an amplitude spectrum. The deterministic problem in a two-term Volterra model (see §6) then consists of solving the second-order wave–body interactions at the sum and difference frequencies for all possible pairs of the incident wave frequency components. These second-order bichromatic problems are to be solved for the requisite sum- and difference-frequency quadratic transfer functions (QTF's) for the forces, pressures, surface elevations, etc. corresponding to unit amplitudes of the incident components. Thus, we extend the formulation and numerical method of KY-I to the general case of bichromatic incident waves. For completeness, we also include the radiation problem and obtain second-order motions, for example for freely floating bodies in irregular waves. As in KY-I, the second-order sum- and difference-frequency potentials are calculated explicitly so that in addition to the corresponding sum- and difference-frequency force and motion QTF's, local behaviours of the flow in the bifrequency domain are also obtained.

The complete sum- and difference-frequency force calculation was first attempted by Loken (1986), although a number of important issues such as those associated with the simple truncation of the free-surface integral were not satisfactorily resolved. For the difference-frequency problem, some improvements were later made by Benshop, Hermans & Huijsmans (1987), Eatock Taylor, Hung & Mitchell (1988), and Matsui (1988), especially in the treatment of the free-surface integral. To avoid solving for the second-order potentials directly, the latter works employed an indirect formulation based on the use of an assisting radiation potential (Molin 1979; Lighthill 1979). Thus only integrated quantities such as forces and moments were obtained for the difference-frequency problem. Furthermore, despite refinements, the convergence of the free-surface integral was typically still only algebraic with truncation distance and consequently relatively large numerical quadrature inner regions were necessary.

With the exception of these works, theoretical and computed results for the general second-order problem are rather scarce. The primary difficulty is clearly the need for the nonlinear (sum- and difference-frequency) potentials and/or the associated forces, etc. With the pressing needs for engineering solutions, a number of approximation methods for the force QTF's have been proposed and widely used in applications. Examples include the methods of Newman (1974), Pinkster (1980), Standing & Dacunha (1982), and Marthinsen (1983) for slowly varying (difference-frequency) wave excitations; and those of De Boom, Pinkster & Tan (1983), Herfjord & Nielsen (1986), and Petrauskas & Liu (1987) for sum-frequency forces. These simplifying approximations are usually justified on heuristic grounds and typically neglect one or more components of the complete second-order forcing. In the absence of a more complete solution, however, the general validity of a specific approximation, and the relative superiority of one method over another have heretofore not been established. These questions are addressed extensively in §5,

where the approximated QTF's are compared to the exact ones for a number of simple geometries.

The mathematical formulation and numerical method for the two-frequency second-order problem generally follow that of KY-I for the monochromatic case. For completeness, an outline is given in §§2–4. For numerical illustration we consider in §5 the diffraction (and radiation) of a uniform vertical circular cylinder of different depths, and also for a fixed and freely floating hemisphere. The complete sum- and difference-frequency QTF's for plane unidirectional bichromatic incident waves of arbitrary frequencies are obtained for the wave excitation, pressure distribution and surface elevations. In addition to systematic convergence tests, the numerical results are also validated against semi-analytic solutions for the case of a uniform vertical circular cylinder which are developed in the Appendix. Given the complete excitation and response QTF's and the incident wave spectrum, the stochastic properties of second-order wave excitations and body responses in Gaussian random seas can be readily calculated. This is briefly introduced in §6.

2. Formulation of the second-order bichromatic problem

We consider the first- and second-order interactions of plane bichromatic incident waves with a large three-dimensional body. Cartesian coordinates with the (x, y)-plane in the quiescent free surface and z positive upward are chosen. Assuming potential flow and weak nonlinearities, we write the total velocity potential Φ as a perturbation series with respect to the wave slope parameter ϵ ($\epsilon \ll 1$):

$$\Phi = \epsilon\Phi^{(1)} + \epsilon^2\Phi^{(2)} + \dots . \tag{2.1a}$$

Using (2.1a), expanding free-surface and body quantities in terms of Taylor series about mean positions, and collecting terms of equal order, the boundary-value problem at each order is linear and we can decompose Φ into the incident (Φ_{I}), diffraction (Φ_{D}), and radiation (Φ_{R}) potentials:

$$\Phi = \epsilon(\Phi_{\mathrm{I}}^{(1)} + \Phi_{\mathrm{D}}^{(1)} + \Phi_{\mathrm{R}}^{(1)}) + \epsilon^2(\Phi_{\mathrm{I}}^{(2)} + \Phi_{\mathrm{D}}^{(2)} + \Phi_{\mathrm{R}}^{(2)}) + \dots . \tag{2.1b}$$

At first order, the diffraction potential, $\Phi_{\mathrm{D}}^{(1)}$, represents the scattered waves due to the presence of a fixed body, while the radiation potential, $\Phi_{\mathrm{R}}^{(1)}$, represents radiated waves due to first-order body motions. A similar decomposition can be made at second order although the choice is in general not unique. A convenient and consistent definition is to let the diffraction potential, $\Phi_{\mathrm{D}}^{(2)}$, represent the combined diffracted potential due to the presence of second-order incident waves as well as the forcing due to *all* the quadratic contributions of first-order quantities on the free surface and on the body (i.e. a second-order problem for a body either fixed or undergoing first-order motions only). The radiation potential, $\Phi_{\mathrm{R}}^{(2)}$, then represents the outgoing waves due to second-order motions only, in the absence of ambient waves or first-order disturbances. This decomposition is consistent with the first-order problem in the sense that $\Phi_{\mathrm{I}}^{(2)}$ and $\Phi_{\mathrm{D}}^{(2)}$ together give the total exciting forces for the second-order motions. Note that under the present decomposition, all the difficult second-order effects are confined to the 'diffraction' problem for $\Phi_{\mathrm{D}}^{(2)}$, while the second-order radiation problem is now identical to that of a first-order problem but at the respective sum and difference frequencies.

In the presence of multiple incident wave components, it is sufficient at second-order to consider the general problem of wave–body interactions for an arbitrary

bichromatic pair of incident components. In the presence of two plane incident waves of frequencies ω_1, ω_2, then, we write for the first-order velocity potential $\Phi^{(1)}$:

$$\Phi^{(1)}(\boldsymbol{x}, t) = \mathrm{Re}\left\{\sum_{j=1}^{2} \phi_j^{(1)}(\boldsymbol{x})\, \mathrm{e}^{-\mathrm{i}\omega_j t}\right\}, \tag{2.2}$$

and the second-order potential as a superposition of sum- and difference-frequency terms:

$$\Phi^{(2)}(\boldsymbol{x}, t) = \mathrm{Re} \sum_{j=1}^{2} \sum_{l=1}^{2} \{\phi^-(\boldsymbol{x})\, \mathrm{e}^{-\mathrm{i}\omega^- t} + \phi^+(\boldsymbol{x})\, \mathrm{e}^{-\mathrm{i}\omega^+ t}\}, \tag{2.3}$$

where $\omega^- = \omega_j - \omega_l$ and $\omega^+ = \omega_j + \omega_l$. The sum- and difference-frequency potentials in (2.3), ϕ^+ and ϕ^-, can be solved independently after separating the forcing terms and the boundary-value problem accordingly.

Assuming unidirectional wave incidence from $x = -\infty$ (say), wave amplitude A_j, $j = 1, 2$, and uniform but arbitrary water depth, h, the first-order incident potential is given by

$$\phi_{\mathrm{I}}^{(1)} = \sum_{j=1}^{2} \frac{-\mathrm{i}gA_j}{\omega_j} \frac{\cosh k_j(z+h)}{\cosh k_j h} \mathrm{e}^{\mathrm{i}k_j x}, \tag{2.4}$$

where the frequency ω_j and wavenumber k_j satisfy the dispersion relationship: $\omega_j^2 = k_j g \tanh(k_j h)$, $j = 1, 2$, g being the gravitational acceleration.

The second-order incident wave potential, $\Phi_{\mathrm{I}}^{(2)}$, satisfies the Laplace equation, no-flux condition on the sea bottom ($z = -h$), and the inhomogeneous free-surface condition on $z = 0$:

$$\left(\frac{\partial}{\partial t^2} + g\frac{\partial}{\partial z}\right) \Phi_{\mathrm{I}}^{(2)} = Q_{\mathrm{II}},$$

where

$$Q_{\mathrm{II}} \equiv \frac{1}{g} \frac{\partial \Phi_{\mathrm{I}}^{(1)}}{\partial t} \frac{\partial}{\partial z}\left(\frac{\partial^2 \Phi_{\mathrm{I}}^{(1)}}{\partial t^2} + g\frac{\partial \Phi_{\mathrm{I}}^{(1)}}{\partial z}\right) - \frac{\partial}{\partial t}(\nabla \Phi_{\mathrm{I}}^{(1)})^2. \tag{2.5}$$

Upon substituting (2.2)–(2.4) into (2.5) and solving for $\Phi_{\mathrm{I}}^{(2)}$, we obtain the sum- and difference-frequency second-order incident wave potentials (e.g. Bowers 1976):

$$\phi_{\mathrm{I}}^+ = \tfrac{1}{2}(\gamma_{jl}^+ + \gamma_{lj}^+) \frac{\cosh k^+(z+h)}{\cosh k^+ h} \mathrm{e}^{\mathrm{i}k^+ x},$$

where

$$\gamma_{jl}^+ = \frac{-\mathrm{i}gA_jA_l}{2\omega_j} \frac{k_j^2(1-\tanh^2 k_j h) + 2k_j k_l(1-\tanh k_j h \tanh k_l h)}{\nu^+ - k^+ \tanh k^+ h}, \tag{2.6}$$

and

$$\phi_{\mathrm{I}}^- = \tfrac{1}{2}(\gamma_{jl}^- + \gamma_{lj}^{-*}) \frac{\cosh k^-(z+h)}{\cosh k^- h} \mathrm{e}^{\mathrm{i}k^- x},$$

where

$$\gamma_{jl}^- = \frac{-\mathrm{i}gA_jA_l^*}{2\omega_j} \frac{k_j^2(1-\tanh^2 k_j h) - 2k_j k_l(1+\tanh k_j h \tanh k_l h)}{\nu^- - k^- \tanh k^- h}. \tag{2.7}$$

In the above equations, an asterisk represents a complex conjugate, and $\nu^\pm$ and $k^\pm$ are defined respectively by

$$\nu^\pm = \omega^{\pm 2}/g, \quad k^\pm = k_j \pm k_l. \tag{2.8}$$

One can easily check from (2.6) that ϕ_{I}^+ vanishes for deep water: $k_j h, k_l h \gg 1$. As the water depth decreases, the magnitude of ϕ_{I}^+ continues to increase, eventually blowing

up as the Ursell number for small kh and the use of Stokes expansion (2.1) becomes restrictive (Ursell 1953). In the limit of a single regular wave, $\omega_j \to \omega_l$, ϕ_{I}^{+} reduces to the well-known second-order uniform Stokes wave:

$$\phi_{\mathrm{I}}^{+} = \frac{-3\mathrm{i}\omega A^2}{8} \frac{\cosh 2k(z+h)}{\sinh^4 kh} \mathrm{e}^{2\mathrm{i}kx}. \tag{2.9}$$

For the difference-frequency incident wave potential, ϕ_{I}^{-}, the contribution is finite in the general deep-water limit $k_j h, k_l h \gg 1$. For water depth large with respect to k_j, k_l but moderate relative to the difference-frequency wavenumber k^-, say, $k^- h = O(1)$, (2.6) gives

$$\phi_{\mathrm{I}}^{-} \sim \frac{-\mathrm{i}A_j A_l^* \omega_j \omega_l}{(\omega_j - \omega_l) - (\omega_j + \omega_l) \tanh k^- h} \frac{\cosh k^-(z+h)}{\cosh k^- h} \mathrm{e}^{\mathrm{i}k^- x}. \tag{2.10a}$$

In the limit of water depth large compared to k^-, $k^- h \gg 1$, the difference-frequency potential has the form:

$$\phi_{\mathrm{I}}^{-} \sim \mathrm{i}A_j A_l^* \frac{(\omega_l - \omega_j)\omega_j \omega_l}{(\omega_j - \omega_l)^2 - |\omega_j^2 - \omega_l^2|} \mathrm{e}^{\nu^- z + \mathrm{i}\nu^- x} \tag{2.10b}$$

In the limit of monochromatic incidence, $\omega_j \to \omega_l$, the difference-frequency incident potential for infinite depth, (2.10b), approaches a finite limit, while (2.10a) becomes essentially a shallow-water wave of $O(\epsilon^2/\omega^-)$, and therefore only valid for small Ursell number.

It is evident that the depth attenuations of second-order incident waves are determined by $k^{\pm}$ respectively for $\phi_{\mathrm{I}}^{\pm}$, so that ϕ_{I}^{-} in general penetrates deeper than ϕ_{I}^{+} especially for small frequency differences. The deep penetration of ϕ_{I}^{-} in narrow-banded seas is of importance to deep-draft bodies.

We now consider the first- and second-order interactions of the bichromatic incident waves with a general three-dimensional freely floating body. For convenience, we define the first-order body disturbance potential, $\phi_{\mathrm{B}}^{(1)}$, as a s sum of the first-order diffraction and radiation potentials: $\phi_{\mathrm{B}}^{(1)} = \phi_{\mathrm{D}}^{(1)} + \phi_{\mathrm{R}}^{(1)}$. This potential satisfies the Laplace equation in the undisturbed fluid volume, zero normal velocity on the bottom, $z = -h$, and the following boundary conditions on the mean free surface, S_{F}, and the mean body position, S_{B}:

$$\left(-\omega^2 + g\frac{\partial}{\partial z}\right)\phi_{\mathrm{B}}^{(1)} = 0 \qquad \text{on } S_{\mathrm{F}}\colon z = 0; \tag{2.11a}$$

$$\frac{\partial \phi_{\mathrm{B}}^{(1)}}{\partial n} = -\frac{\partial \phi_{\mathrm{I}}^{(1)}}{\partial n} - \mathrm{i}\omega \boldsymbol{n} \cdot (\boldsymbol{\xi}^{(1)} + \boldsymbol{\alpha}^{(1)} \times \boldsymbol{r}) \quad \text{on } S_{\mathrm{B}}; \tag{2.11b}$$

plus a Sommerfeld radiation condition at infinity, S_∞:

$$\lim_{\rho \to \infty} \rho^{\frac{1}{2}} \left(\frac{\partial}{\partial \rho} - \mathrm{i}k\right)\phi_{\mathrm{B}}^{(1)} = 0 \qquad \text{on } S_\infty. \tag{2.11c}$$

In (2.11), $\boldsymbol{r}$ represents the position vector on the body surface, ρ the radial distance from the origin, $\rho^2 = x^2 + y^2$, and $\boldsymbol{n} = (n_x, n_y, n_z)$ the outward unit normal vector for the fluid. The first term on the right-hand side of the body boundary condition (2.11b) is associated with the diffraction potential, $\phi_{\mathrm{D}}^{(1)}$, and the second term with the

radiation problem, $\phi_R^{(1)}$. The translational (Ξ) and rotational (α) first-order motions in the presence of two incident wave frequencies have the forms

$$\Xi^{(1)}(x,t) = \mathrm{Re}\sum_{j=1}^{2}[\xi_j^{(1)}(x)\,e^{-i\omega_j t}], \quad \xi_j^{(1)} = (\xi_{xj}^{(1)}, \xi_{yj}^{(1)}, \xi_{zj}^{(1)}), \tag{2.12a}$$

$$\alpha^{(1)}(x,t) = \mathrm{Re}\sum_{j=1}^{2}[\alpha_j^{(1)}(x)\,e^{-i\omega_j t}], \quad \alpha_j^{(1)} = (\alpha_{xj}^{(1)}, \alpha_{yj}^{(1)}, \alpha_{zj}^{(1)}), \tag{2.12b}$$

where the subscripts x, y, and z denote the translational and rotational modes with respect to the x-, y-, and z-axis, respectively.

The solution for the first-order problem (2.11) is now classical and will not be further elaborated. The first-order potentials and motions are necessary to specify the inhomogeneous free-surface and body boundary condition forcing terms for the second-order problem. The inhomogeneous free-surface condition for the total second-order potential, $\Phi^{(2)}$, is given by (2.5) with $\Phi_I^{(1)}$ replaced by $\Phi^{(1)}$. The second-order body boundary condition can likewise be obtained by writing Taylor series expansions for the relevant variables on the instantaneous body surface with respect to the mean body position, S_B (e.g. Ogilvie 1983). We define the second-order diffraction potential, $\Phi_D^{(2)}$, to be the solution of the boundary-value problem containing both the inhomogeneous free-surface and body-surface boundary conditions, i.e. a diffraction problem containing the quadratic contributions of *all* the first-order waves plus the second-order incident wave but in the absence of second-order motions. The free-surface and body boundary conditions for $\Phi_D^{(2)}$ on the respective mean positions are

$$\left(\frac{\partial}{\partial t^2}+g\frac{\partial}{\partial z}\right)\Phi_D^{(2)} = Q \quad \text{on } S_F\colon z=0,$$

where

$$Q \equiv \frac{1}{g}\frac{\partial\Phi^{(1)}}{\partial t}\frac{\partial}{\partial z}\left(\frac{\partial^2\Phi^{(1)}}{\partial t^2}+g\frac{\partial\Phi^{(1)}}{\partial z}\right)-\frac{\partial}{\partial t}(\nabla\Phi^{(1)})^2-Q_{II}; \tag{2.13}$$

and

$$\frac{\partial\Phi_D^{(2)}}{\partial n} = -\frac{\partial\Phi_I^{(2)}}{\partial n}+B \quad \text{on } S_B,$$

where

$$B \equiv n\cdot\left(\frac{\partial H}{\partial t}r\right)-n\cdot[(\Xi^{(1)}+\alpha^{(1)}\times r)\cdot\nabla]\nabla\Phi^{(1)}+(\alpha^{(1)}\times n)\cdot[V^{(1)}-\nabla\Phi^{(1)}]. \tag{2.14}$$

In (2.14), $V^{(i)} \equiv \partial/\partial t(\Xi^{(i)}+\alpha^{(i)}\times r), i=1,2$, and H is a matrix whose elements are second order and are the quadratic products of the first-order rotational motions:

$$H = -\tfrac{1}{2}\begin{bmatrix}(\alpha_y^2+\alpha_z^2) & 0 & 0\\ -2\alpha_x\alpha_y & (\alpha_x^2+\alpha_z^2) & 0\\ -2\alpha_x\alpha_z & -2\alpha_y\alpha_z & (\alpha_x^2+\alpha_y^2)\end{bmatrix}. \tag{2.15}$$

As pointed out by Ogilvie (1983), the expression of the H-matrix depends on the sequence of rotations. For (2.15) the order roll-pitch-yaw (4-5-6) is used. In the absence of first-order rotational motions, the body forcing term B in (2.14) is simplified:

$$B(x,t) = -n\cdot(\Xi^{(1)}\cdot\nabla)\nabla\Phi^{(1)}. \tag{2.16}$$

Since the free-surface and body-surface forcing terms Q and B in (2.13) and (2.14)

are quadratic products of first-order bichromatic quantities, they can be written in the form

$$[Q,B](\boldsymbol{x},t) = \mathrm{Re}\sum_{j=1}^{2}\sum_{l=1}^{2}\{[Q^+,B^+](\boldsymbol{x})\,\mathrm{e}^{-\mathrm{i}\omega^+ t}+[Q^-,B^-](\boldsymbol{x})\,\mathrm{e}^{-\mathrm{i}\omega^- t}\}. \tag{2.17}$$

The sum- and difference-frequency components respectively of the second-order diffraction potential, $\phi_{\mathrm{D}}^{\pm}$, then satisfy the following boundary value problems which can be solved independently:

$$\nabla^2\phi_{\mathrm{D}}^{\pm} = 0 \quad \text{in the quiescent fluid volume } (z<0); \tag{2.18a}$$

$$\left(-\omega^{\pm 2}+g\frac{\partial}{\partial z}\right)\phi_{\mathrm{D}}^{\pm} = Q^{\pm} \quad \text{on } S_{\mathrm{F}}\colon z=0; \tag{2.18b}$$

$$\frac{\partial\phi_{\mathrm{D}}^{\pm}}{\partial z} = 0 \quad \text{on } z=-h; \tag{2.18c}$$

$$\frac{\partial\phi_{\mathrm{D}}^{\pm}}{\partial n} = -\frac{\partial\phi_{\mathrm{I}}^{\pm}}{\partial n}+B^{\pm} \quad \text{on } S_{\mathrm{B}}; \tag{2.18d}$$

$$\text{condition at infinity} \quad \text{on } S_{\infty} \quad (\rho\to\infty). \tag{2.18e}$$

In (2.18*b*), the sum- and difference-frequency free-surface forcing terms can be written in symmetric forms as follows:

$$Q^+ = \tfrac{1}{2}(q_{jl}^+ + q_{lj}^+), \quad Q^- = \tfrac{1}{2}(q_{jl}^- + q_{lj}^{-*}); \tag{2.19}$$

where

$$q_{jl}^+ = \frac{-\mathrm{i}\omega_l}{2g}\phi_l^{(1)}\left(-\omega_j^2\frac{\partial\phi_j^{(1)}}{\partial z}+g\frac{\partial^2\phi_j^{(1)}}{\partial z^2}\right)+\mathrm{i}\omega_l\nabla\phi_j^{(1)}\cdot\nabla\phi_l^{(1)}-q_{\mathrm{II}\,jl}^+, \tag{2.20}$$

$$q_{jl}^- = \frac{\mathrm{i}\omega_l}{2g}\phi_l^{(1)*}\left(-\omega_j^2\frac{\partial\phi_j^{(1)}}{\partial z}+g\frac{\partial^2\phi_j^{(1)}}{\partial z^2}\right)-\mathrm{i}\omega_l\nabla\phi_j^{(1)}\cdot\nabla\phi_l^{(1)*}-q_{\mathrm{II}\,jl}^-. \tag{2.21}$$

The sum- and difference-frequency components of the body-surface forcing term B in (2.14) can be written in similar forms. Equation (2.16), for example, has the form:

$$B^+ = \tfrac{1}{2}(b_{jl}^+ + b_{lj}^+), \quad B^- = \tfrac{1}{2}(b_{jl}^- + b_{lj}^{-*}); \tag{2.22}$$

where

$$b_{jl}^+ = -\tfrac{1}{2}\boldsymbol{n}\cdot(\boldsymbol{\xi}_l^{(1)}\cdot\nabla)\nabla\phi_j^{(1)} \tag{2.23}$$

$$b_{jl}^- = -\tfrac{1}{2}\boldsymbol{n}\cdot(\boldsymbol{\xi}_l^{(1)*}\cdot\nabla)\nabla\phi_j^{(1)}. \tag{2.24}$$

Finally, for the second-order radiation problem, $\phi_{\mathrm{R}}^{\pm}$ satisfy the boundary-value problems similar to that given by (2.11) (for $\phi_{\mathrm{R}}^{(1)}$) but substituting $\omega^{\pm}$ for ω and $k_2^{\pm}$ for k (where $k_2^{\pm}$ are the wavenumbers associated with $\omega^{\pm}$), and the body boundary condition due to second-order motions:

$$\frac{\partial\phi_{\mathrm{R}}^{\pm}}{\partial n} = -\mathrm{i}\omega^{\pm}\boldsymbol{n}\cdot(\boldsymbol{\xi}^{\pm}+\boldsymbol{\alpha}^{\pm}\times\boldsymbol{r}) \quad \text{on } S_{\mathrm{B}}. \tag{2.25}$$

The second-order motions, $\boldsymbol{\Xi}^{(2)}$ and $\boldsymbol{\alpha}^{(2)}$, being written in the form

$$[\boldsymbol{\Xi}^{(2)},\boldsymbol{\alpha}^{(2)}](\boldsymbol{x},t) = \mathrm{Re}\sum_{j=1}^{2}\sum_{l=1}^{2}\{[\boldsymbol{\xi}^+,\boldsymbol{\alpha}^+](\boldsymbol{x})\,\mathrm{e}^{-\mathrm{i}\omega^+ t}+[\boldsymbol{\xi}^-,\boldsymbol{\alpha}^-](\boldsymbol{x})\,\mathrm{e}^{-\mathrm{i}\omega^- t}\}. \tag{2.26}$$

Thus the solution of $\phi_{\mathrm{R}}^{\pm}$ for the second-order hydrodynamic coefficients, say, is identical to that of a first-order radiation problem at the sum and difference frequencies.

With the exception of the radiation condition (2.18*e*) for $\phi_{\mathrm{D}}^{\pm}$, the boundary-value problems for the second-order potentials are now complete. For monochromatic incident waves, an appropriate radiation condition for the double-frequency second-order potential was first obtained by Molin (1979) and adopted in KY-I. For the general bichromatic problem, the analysis can be extended in a straightforward way. Following Molin, we decompose $\phi_{\mathrm{D}}^{\pm}$, governed by the linear boundary-value problem (2.18), into a homogeneous, $\phi_{\mathrm{H}}^{\pm}$, and particular solution, $\phi_{\mathrm{P}}^{\pm}$, satisfying respectively the homogeneous and inhomogeneous free-surface conditions and jointly the inhomogeneous body-boundary condition. The homogeneous potential, $\phi_{\mathrm{H}}^{\pm}$, then has the far-field behaviour of a free propagating wave:

$$\phi_{\mathrm{H}}^{\pm} \sim \frac{\mathrm{e}^{\mathrm{i}k_2^{\pm}\rho}}{\rho^{\frac{1}{2}}} + O(\rho^{-\frac{3}{2}}), \quad \rho \gg 1. \tag{2.27}$$

The asymptotic behaviour of the particular potential, $\phi_{\mathrm{P}}^{\pm}$, is governed by that of the free-surface forcing, $Q^{\pm}$. $Q^{\pm}$ contain all quadratic combinations of the first-order incident (I) and body disturbance (diffracted and radiated) (B) waves and may be represented symbolically as Q_{IB} and Q_{BB}. From the first-order potentials, we have

$$\phi_{\mathrm{B}j}^{(1)} \sim \mathrm{e}^{\mathrm{i}k_j\rho}\rho^{-\frac{1}{2}} + O(\rho^{-\frac{3}{2}}), \quad \rho \gg 1; \tag{2.28a}$$

$$\phi_{\mathrm{I}j}^{(1)} \sim \mathrm{e}^{\mathrm{i}k_j\rho\cos\theta}; \tag{2.28b}$$

so that $Q_{\mathrm{BB}}^{\pm} \sim \rho^{-1}$, for $\rho \gg 1$, and the far-field behaviour of $Q^{\pm}$ is dominated by Q_{IB} which has the asymptotic form

$$Q_{\mathrm{IB}}^{\pm} \sim \mathrm{e}^{\mathrm{i}\rho(k_j \pm k_l\cos\theta)}\rho^{-\frac{1}{2}} + O(\rho^{-1}), \quad \rho \gg 1. \tag{2.29}$$

Thus, to leading order, $O(\rho^{-\frac{1}{2}})$, the inhomogeneous second-order potential has the far-field behaviour

$$\phi_{\mathrm{P}}^{\pm} \sim E_{jl}^{\pm}(\theta, z)\,\mathrm{e}^{\mathrm{i}\rho(k_j \pm k_l\cos\theta)}\rho^{-\frac{1}{2}} + O(\rho^{-1}). \tag{2.30}$$

Satisfying the Laplace equation to leading order, and the bottom boundary condition, $E^{\pm}$ has the form

$$E_{jl}^{\pm}(\theta, z) = \Theta_{jl}^{\pm}(\theta)\cosh\{(k_j^2 + k_l^2 \pm 2k_j k_l\cos\theta)^{\frac{1}{2}}(z+h)\}. \tag{2.31}$$

Finally, $\Theta(\theta)$ can be obtained from the free-surface condition of $\phi_{\mathrm{P}}^{\pm}$. Equations (2.27), (2.30) are direct generalizations of the results of Molin (1979), and in the special case of monochromatic waves, $\omega_j = \omega_l$, reduce identically to those of Molin (1979). These results can also be derived starting from the initial-value problem and considering the long-time limit (cf. Wang 1987). It is of interest to note that the depth attenuation factors in (2.31) are angular dependent and have a minimum when $k_j = k_l$ and $\theta = \pi$ for the sum-frequency problem, and when $\theta = 0$ for difference-frequency problem.

3. A boundary-integral equation method for the sum- and difference-frequency second-order potentials

We solve the first- and second-order boundary-value problems of §2 by a boundary-integral equation method using free-surface wave-source Green functions. Consider first the boundary-value problem (2.18) for the second-order diffraction potentials, $\phi_{\mathrm{D}}^{\pm}$. Introducing the sum- and difference-frequency linear wave-source

potentials, $G^{\pm}$, at frequencies $\omega^{\pm}$, and applying Green's identity to $\phi_{\mathrm{D}}^{\pm}$ and $G^{\pm}$, we obtain a Fredholm integral equation of the second kind for $\phi_{\mathrm{D}}^{\pm}$:

$$2\pi\phi_{\mathrm{D}}^{\pm}+\iint_{S_{\mathrm{B}}}\phi_{\mathrm{D}}^{\pm}\frac{\partial G^{\pm}}{\partial n}\,\mathrm{d}S=\iint_{S_{\mathrm{B}}}G^{\pm}\left\{B^{\pm}-\frac{\partial\phi_{\mathrm{I}}^{\pm}}{\partial n}\right\}\mathrm{d}S+\frac{1}{g}\iint_{S_{\mathrm{F}}}Q^{\pm}G^{\pm}\,\mathrm{d}S. \tag{3.1}$$

The forcing terms $B^{\pm}$ and $Q^{\pm}$, on the right-hand side are given in terms of solutions of the first-order problem and assumed known. In deriving (3.1), use is made of the so-called 'weak' radiation condition which states that the integral at infinity (on S_{∞}) vanishes. This can be shown using the method of stationary phase and the known far-field asymptotic behaviour of $\phi_{\mathrm{D}}^{\pm}$ ((2.27) *et seq*) and of $G^{\pm}$.

For computational expediency, we consider a body with a vertical axis of symmetry. In this case, (3.1) can be integrated with respect to θ to obtain a sequence of one-dimensional integral equations for each angular Fourier mode. Specifically, we expand $\phi_{\mathrm{D}}^{\pm}$, $Q^{\pm}$, $B^{\pm}$ and $G^{\pm}$ in terms of Fourier cosine series:

$$[\phi_{\mathrm{D}}^{\pm}(\rho,\theta,z),Q^{\pm}(\rho,\theta),B^{\pm}(\rho,\theta,z)]=\sum_{n=0}^{\infty}[\phi_{\mathrm{D}n}^{\pm}(\rho,z),Q_n^{\pm}(\rho),B_n^{\pm}(\rho,z)]\cos n\theta; \tag{3.2a}$$

$$G^{\pm}(\rho,\theta,z;\rho',\theta',z')=\sum_{n=0}^{\infty}\frac{\epsilon_n}{2\pi}G_n^{\pm}(\rho,z;\rho',z')\cos n(\theta-\theta'); \tag{3.2b}$$

where $\epsilon_n=1$ for $n=0$ and $\epsilon_n=2$ for $n\geqslant 1$. Substituting (3.2) into (3.1) and using orthogonality of the trigonometric functions, we obtain, after integration in θ, a sequence of one-dimensional integral equations in the (ρ,z)-plane:

$$2\pi\phi_{\mathrm{D}n}^{\pm}+\int_{\partial_{\mathrm{B}}}\rho\,\mathrm{d}l\,\phi_{\mathrm{D}n}^{\pm}\frac{\partial G_n^{\pm}}{\partial n}=\int_{\partial_{\mathrm{B}}}\rho\,\mathrm{d}l\left(B_n^{\pm}-\frac{\partial\phi_{\mathrm{I}n}^{\pm}}{\partial n}\right)G_n^{\pm}+\frac{1}{g}\int_{\partial_{\mathrm{F}}}\rho\,\mathrm{d}\rho\,Q_n^{\pm}\,G_n^{\pm}, \tag{3.3}$$

where the line integrals are along the traces $\partial_{\mathrm{B}},\partial_{\mathrm{F}}$ of S_{B} and S_{F} respectively. Rearranging the double products of Fourier series for (2.20), the nth mode sum-frequency free-surface forcing term Q_n^{+} in (3.3) has the form

$$\begin{aligned}q_{0jl}^{+}=\frac{-\mathrm{i}g^2A_jA_lk_j^2}{2\omega_j}\sum_{m=0}^{\infty}\frac{2}{\epsilon_m}\Bigg[&\left(\frac{\tanh k_j^2h}{2}+\frac{k_l}{k_j}\tanh k_jh\tanh k_lh\right.\\&\left.+\frac{k_l}{k_j}\frac{\epsilon_m}{2}\frac{m^2}{(k_j\rho)(k_l\rho)}\right)\psi_m^j\psi_m^l-\frac{1}{2}\frac{\partial^2\psi_m^j}{\partial(k_jz)^2}\psi_m^l+\frac{k_l}{k_j}\frac{\partial\psi_m^j}{\partial(k_j\rho)}\frac{\partial\psi_m^l}{\partial(k_l\rho)}\Bigg]\Bigg|_{z=0},\end{aligned} \tag{3.4a}$$

$$\begin{aligned}q_{njl}^{+}=\frac{-\mathrm{i}g^2A_jA_lk_j^2}{2\omega_j}\Bigg[&\sum_{m=0}^{n}\left\{\chi_{jl}\psi_{n-m}^j\psi_m^l-\frac{1}{2}\frac{\partial^2\psi_{n-m}^j}{\partial(k_jz)^2}\psi_m^l+\frac{k_l}{k_j}\frac{\partial\psi_{n-m}^j}{\partial(k_j\rho)}\frac{\partial\psi_m^l}{\partial(k_l\rho)}\right\}\\&+\sum_{m=0}^{\infty}\left\{\hat{\chi}_{jl}(\psi_{n+m}^j\psi_m^l+\psi_m^j\psi_{n+m}^l)-\frac{1}{2}\left(\frac{\partial^2\psi_{n+m}^j}{\partial(k_jz)^2}\psi_m^l+\frac{\partial^2\psi_m^j}{\partial(k_jz)^2}\psi_{n+m}^l\right)\right.\\&\left.+\frac{k_l}{k_j}\left(\frac{\partial\psi_{n+m}^j}{\partial(k_j\rho)}\frac{\partial\psi_m^l}{\partial(k_l\rho)}+\frac{\partial\psi_m^j}{\partial(k_j\rho)}\frac{\partial\psi_{n+m}^l}{\partial(k_l\rho)}\right)\right\}\Bigg]\Bigg|_{z=0},\end{aligned} \tag{3.4b}$$

where

$$\begin{Bmatrix}\chi_{jl}\\ \hat{\chi}_{jl}\end{Bmatrix}=\frac{\tanh^2k_jh}{2}+\frac{k_l}{k_j}\tanh k_jh\tanh k_lh\mp\frac{k_l}{k_j}\frac{(n\mp m)\,m}{(k_j\rho)(k_l\rho)}. \tag{3.5}$$

In the above equations, ψ_m^j represents the mth Fourier mode of the total first-order potential of frequency ω_j and normalized by $-\mathrm{i}gA_j/\omega_j$, and the free-surface condition for ψ has been exploited in deriving (3.4). The nth mode difference-frequency free-surface forcing, Q_n^{-}, can be obtained in a similar way using (3.2) and (2.21).

For the body forcing terms, the sum- and difference-frequency components must also be expressed in terms of circumferential modes. In the absence of rotational modes, the sum-frequency body-boundary forcing term (2.23) has the following expression:

$$-2b_{jl}^{+} = n_\rho\left(\xi_{\rho l}^{(1)}\frac{\partial^2\phi_j^{(1)}}{\partial\rho^2}+\frac{\xi_{\theta l}^{(1)}}{\rho}\frac{\partial^2\phi_j^{(1)}}{\partial\rho\,\partial\theta}+\xi_{zl}^{(1)}\frac{\partial^2\phi_j^{(1)}}{\partial\rho\,\partial z}\right) + n_z\left(\xi_{\rho l}^{(1)}\frac{\partial^2\phi_j^{(1)}}{\partial z\,\partial\rho}+\frac{\xi_{\theta l}^{(1)}}{\rho}\frac{\partial^2\phi_j^{(1)}}{\partial z\,\partial\theta}+\xi_{zl}^{(1)}\frac{\partial^2\phi_j^{(1)}}{\partial z^2}\right), \quad (3.6)$$

where the unit outward normal vector to ∂_B is given by $\boldsymbol{n} = (n_\rho, n_z)$. Substituting $\xi_\rho^{(1)} = \xi_x^{(1)}\cos\theta$, $\xi_\theta^{(1)} = -\xi_x^{(1)}\sin\theta$, and setting $\xi_y^{(1)}$ to be zero without loss of generality the Fourier components of (3.6) are obtained to be

$$b_{0jl}^{+} = -\frac{\xi_{xl}^{(1)}}{4}\left[n_\rho\frac{\partial^2\phi_{1j}^{(1)}}{\partial\rho^2}+n_z\frac{\partial^2\phi_{1j}^{(1)}}{\partial z\,\partial\rho}+\frac{1}{\rho}\frac{\partial\phi_{1j}^{(1)}}{\partial n}\right]-\frac{\xi_{zl}^{(1)}}{2}\left[n_\rho\frac{\partial^2\phi_{0j}^{(1)}}{\partial\rho\,\partial z}+n_z\frac{\partial^2\phi_{0j}^{(1)}}{\partial z^2}\right], \quad (3.7)$$

$$b_{njl}^{+} = -\frac{\xi_{xl}^{(1)}}{4}\left[n_\rho\left(\frac{\partial^2\phi_{n-1j}^{(1)}}{\partial\rho^2}+\frac{\partial^2\phi_{n+1j}^{(1)}}{\partial\rho^2}\right)+n_z\left(\frac{\partial^2\phi_{n-1j}^{(1)}}{\partial z\,\partial\rho}+\frac{\partial^2\phi_{n+1j}^{(1)}}{\partial z\,\partial\rho}\right) - \frac{n-1}{\rho}\frac{\partial\phi_{n-1j}^{(1)}}{\partial n}+\frac{n+1}{\rho}\frac{\partial\phi_{n+1j}^{(1)}}{\partial n}\right]-\frac{\xi_{zl}^{(1)}}{2}\left[n_\rho\frac{\partial^2\phi_{nj}^{(1)}}{\partial\rho\,\partial z}+n_z\frac{\partial^2\phi_{nj}^{(1)}}{\partial z^2}\right], \quad (3.8)$$

Corresponding results in the presence of rotational motions can be obtained in a similar way.

The general-order ring sources in (3.3) are calculated from Fourier integrals of the three-dimensional Green function:

$$G_n^{\pm}(\rho,z;\rho',z') = \int_0^{2\pi} G^{\pm}(\rho,z;\rho',z';\cos(\theta-\theta'))\cos(n(\theta-\theta'))\,\mathrm{d}(\theta-\theta'). \quad (3.9)$$

Details of the evaluation of $G_n^{\pm}$, $G_n^{\pm}/\partial n$ and analyses of their asymptotic properties are given in KY-I.

For the present second-order diffraction problem, the so-called Green's theorem integral equation (3.1) is used in favour of a source distribution formulation (e.g. Loken 1986). This has a significant computational advantage in that an additional free-surface integral term (of the form $Q^{\pm}\,\partial G^{\pm}/\partial n$) is avoided. For the first-order problem, however, the use of a source distribution method reduces the order of the spatial derivatives of the Green function by one in the evaluation of the requisite velocity and gradient of velocity terms, and is preferred. This is confirmed in numerical tests where the source method is found to yield more accurate and robust calculations of the derivatives of the potential. Thus for the first-order problem, we write

$$\phi_{Bn}^{(1)}(\boldsymbol{x}) = \int_{\partial_B} \mathrm{d}l'\rho'\sigma_{Bn}(\boldsymbol{x}')\,G_n(\boldsymbol{x};\boldsymbol{x}'), \quad (3.10)$$

where $\sigma_{Bn} = \sigma_{Dn}+\sigma_{Rn}$ are the general-order ring-source strengths for the first-order body disturbance potential.

The numerical solution of the second-order diffraction problem given by the second-kind Fredholm integral solution (3.3) (as well as that resulting from (3.10) for the first-order problem) follow the standard procedure of discretizing ∂_B into linear segments, assuming constant potential (or source strength) over each segment, and collocating at the midpoint of each segment to obtain a system of linear algebraic

equations for the unknown segment potentials (or source strengths). The analytically and computationally difficult task in the solution of (3.3) is the evaluation of the right-hand-side terms, particularly the slowly convergent integral on the unbounded free surface. From the far-field behaviours of $Q^{\pm}$ and $G^{\pm}$, it is evident that the free-surface integral in (3.1) diminishes only as $\rho^{-\frac{1}{2}}$ for $\rho \gg 1$. Direct numerical quadrature in the interior after a simple truncation of this integral (e.g. Loken 1986) is computationally prohibitive and the solutions are unreliable, especially for sum-frequency problems. On the other hand, a moving average technique (e.g. Molin & Marion 1986) is ineffective for bichromatic waves because of non-uniform oscillations of the integrand. For monochromatic waves, an accurate and efficient evaluation of this free-surface integral was obtained in KY-I by an exact analytic integration in the entire local-wave-free domain. The convergence with increasing radius of the region requiring numerical quadrature is subsequently exponentially rapid, resulting in a very compact discretized domain. This method is generalized here to the bichromatic sum- and difference-frequency problems.

Consider the integral

$$I_n(\rho', z') = \frac{1}{g}\int_a^{\infty} \mathrm{d}\rho\, \rho Q_n^{\pm}(\rho)\, G_n^{\pm}(\rho, z=0; \rho', z'), \tag{3.11}$$

where a is the radius of the waterplane of the body. The free-surface forcing terms, $Q_n^{\pm}$, are given in terms of quadratic products of first-order potentials and their derivatives, which may be obtained through (3.10) and its derivatives. In the present method, we evaluate integral (3.11) in two intervals, (a, b) and (b, ∞), where the partition radius b is chosen so that the latter interval is entirely free of local or evanescent waves:

$$I_n = \frac{1}{g}\left[\int_a^b \mathrm{d}\rho\, \rho Q_n^{\pm}\, G_n^{\pm} + \int_b^{\infty} \mathrm{d}\rho\, \rho \hat{Q}_n^{\pm}\, \hat{G}_n^{\pm}\right], \tag{3.12}$$

where $\hat{}$ represents quantities containing propagating wave components only. In practice, the first integral is performed by direct numerical quadrature (say Romberg integration) while the second integral is evaluated analytically. The partition radius b is in general not sensitive to frequency but depends primarily on water depth h. Using the expression of John (1950) for the Green function, and Graf's addition theorem for Bessel functions, we obtain after some algebra the local-wave-free modal amplitudes:

$$\hat{G}_n^{\pm} = -4\pi^2 \mathrm{i} c^{\pm} \cosh k_2^{\pm}(z+h) \cosh k_2^{\pm}(z'+h)\, J_n(k_2^{\pm}\rho')\, H_n(k_2^{\pm}\rho), \tag{3.13}$$

$$\hat{q}_{0jl}^{\pm} = \frac{-\mathrm{i}g^2 A_j A_l k_j^2}{2\omega_j} \sum_{m=0}^{\infty} \frac{2}{\epsilon_m}\left[\left(\Lambda_{jl} + \frac{\epsilon_m k_l}{2k_j}\frac{m^2}{k_j \rho k_l \rho}\right) S_{m,m}^{+j,l} + \frac{k_l}{k_j} T_{m,m}^{+j,l}\right], \tag{3.14}$$

$$\begin{aligned}\hat{q}_{njl}^{+} = \frac{-\mathrm{i}g^2 A_j A_l k_j^2}{2\omega_j}\Bigg\{ &\sum_{m=0}^{n}\left[\left(\Lambda_{jl} - \frac{k_l}{k_j}\frac{(n-m)\,m}{k_j \rho k_l \rho}\right) S_{n-m,m}^{+j,l} + \frac{k_l}{k_j} T_{n-m,m}^{+j,l}\right] \\ &+ \sum_{m=0}^{\infty}\left[\left(\Lambda_{jl} + \frac{k_l}{k_j}\frac{(n+m)\,m}{k_j \rho k_l \rho}\right)(S_{n+m,m}^{+j,l} + S_{m,n+m}^{+j,l}) + \frac{k_l}{k_j}(T_{n+m,m}^{+j,l} + T_{m,n+m}^{+j,l})\right]\Bigg\},\end{aligned} \tag{3.15}$$

where

$$\Lambda_{jl} = \frac{\tanh^2 k_j h}{2} + \frac{k_l}{k_j}\tanh k_j h \tanh k_l h - \tfrac{1}{2}, \tag{3.16}$$

$$S_{K,m}^{+j,l} = (\alpha_K^j \alpha_m^l + \alpha_K^j \beta_m + \beta_K \alpha_m^l) H_K^j H_m^l + \alpha_K^j \beta_m H_K^j H_m^{l*} + \beta_K \alpha_m^l H_K^{j*} H_m^l, \tag{3.17}$$

$$T^{+j,l}_{K,m} = (\alpha^j_K \alpha^l_m + \alpha^j_K \beta_m + \beta_K \alpha^l_m) H^{j'}_K H^{l'}_m + \alpha^j_K \beta_m H^{j'}_K H^{l'*}_m + \beta_K \alpha^l_m H^{j'*}_K H^{l'}_m. \tag{3.18}$$

In the above, J^j_m and H^j_m are respectively the Bessel and Hankel functions of the first kind of order m and argument $k_j\rho$, and a prime denotes differentiation with respect to the argument. The coefficients α and β are given by

$$\alpha^j_K = -4\pi^2 \mathrm{i} c_j \cosh k_j h L^j_K, \quad \beta_K = \tfrac{1}{2}\epsilon_K \mathrm{i}^K. \tag{3.19}$$

The function L^j_n is the nth mode (generalized) Kochin function of frequency ω_j, which describes the far-field behaviour of the first-order disturbance potential in (3.10), and is given by

$$L^j_n = \int_{\partial_B} \mathrm{d}l' \rho' \sigma^j_n(\boldsymbol{x}') J_n(k_j\rho') \cosh k_j(z'+h). \tag{3.20}$$

The coefficient c in (3.19) is defined to be $c = (\nu^2 - k^2)/(k^2 h - \nu^2 h + \nu)$; where $\nu \equiv \omega^2/g$. The constants $c^{\pm}$ in (3.13) are given by the same expression but with ν and k replaced by $\nu^{\pm}$ and $k^{\pm}_2$ respectively. From (3.13) and (3.15) it is evident that the local-wave-free integrand, $\rho \hat{Q}_n \hat{G}_n$, can be expressed as a sum of triple products of Hankel functions (and powers of ρ), and the far-field integral itself in terms of elementary integrals of the form

$$I_1 = \int_b^\infty \mathrm{d}\rho\, \rho^s H_K(k_j\rho) H_m(k_l\rho) H_n(k^{\pm}_2\rho) \quad (s = 0, \pm 1). \tag{3.21}$$

A method for the accurate and efficient evaluation of highly oscillatory and slowly convergent integrals, such as I_1, using Chebyshev expansions of Hankel functions and generalized Fresnel integrals is developed in KY-I. This method is extended here for arbitrary frequency combinations. Note that in the asymptotic expansions for large arguments, the slow convergence of the Hankel function for small k^-_2 in (3.21) is offset by the corresponding favourable asymptotic behaviour of $J_n(k^-_2\rho')$ (see (3.13)).

In addition to the analytic integration of the local-wave-free propagating field, another significant saving in evaluating the outer-field free-surface integral is in the *separation* of the source and field variables by the use of Graf's addition theorem. As a result, we can simultaneously obtain all the terms for every collocation point on the body after calculating the relevant free-surface integral once. This results in a dramatic reduction in computational effort especially for large-scale problems.

4. Sum- and difference-frequency quadratic transfer functions (QTF's)

After solving for the sum- and difference-frequency second-order potentials, the associated second-order forces and moments as well as local pressure, velocities and free-surface elevations can be obtained directly. Following §2, we expand the hydrodynamic pressure, $P(t)$, and free-surface elevation, $\zeta(t)$, also in perturbation series in ϵ. The first- and second-order terms are given respectively by

$$P^{(1)} = -\rho_0 \frac{\partial \Phi^{(1)}}{\partial t}, \quad P^{(2)} = -\rho_0 \frac{\partial \Phi^{(2)}}{\partial t} - \tfrac{1}{2}\rho_0 (\nabla \Phi^{(1)})^2; \tag{4.1}$$

$$\zeta^{(1)} = \frac{-1}{g} \frac{\partial \Phi^{(1)}}{\partial t}\bigg|_{z=0}, \quad \zeta^{(2)} = \frac{-1}{2g} (\nabla \Phi^{(1)})^2 + \frac{1}{g^2} \frac{\partial \Phi^{(1)}}{\partial t} \frac{\partial^2 \Phi^{(1)}}{\partial t \partial z} - \frac{1}{g} \frac{\partial \Phi^{(2)}}{\partial t}\bigg|_{z=0}. \tag{4.2}$$

In the presence of bichromatic waves, the second-order terms in (4.1) and (4.2) can be written in the form

$$(P^{(2)}(t), \zeta^{(2)}(t)) = \mathrm{Re} \sum_{j=1}^{2} \sum_{l=1}^{2} [A_j A_l (p_{jl}^{+}, \eta_{jl}^{+}) \, \mathrm{e}^{-\mathrm{i}\omega^{+}t} + A_j A_l^{*} (p_{jl}^{-}, \eta_{jl}^{-}) \, \mathrm{e}^{-\mathrm{i}\omega^{-}t}], \quad (4.3a)$$

where $p_{jl}^{\pm}$ and $\eta_{jl}^{\pm}$ are now defined as the sum- and difference-frequency quadratic transfer functions for the pressure and free-surface elevation respectively. The complete second-order pressure and elevation QTF's in general contain two separate contributions: (i) that due to quadratic products of first-order potentials, which we denote by p_{q} and η_{q} respectively; and (ii) that due to the second-order potential itself, which we denote by p_{p} and η_{p}:

$$(p_{jl}^{\pm}, \eta_{jl}^{\pm}) = (p_{\mathrm{q}jl}^{\pm}, \eta_{\mathrm{q}jl}^{\pm}) + (p_{\mathrm{p}jl}^{\pm}, \eta_{\mathrm{p}jl}^{\pm}). \quad (4.3b)$$

These components for the sum-frequency case are given by

$$p_{\mathrm{q}jl}^{+} = [-\tfrac{1}{4}\rho_0 \nabla\phi_j^{(1)} \cdot \nabla\phi_l^{(1)}]/A_j A_l, \quad p_{\mathrm{p}jl}^{+} = \rho_0 \, \mathrm{i}\omega^{+}\phi^{+}/A_j A_l, \quad (4.4)$$

$$\eta_{\mathrm{q}jl}^{+} = \left[-\frac{1}{4g}\nabla\phi_j^{(1)} \cdot \nabla\phi_l^{(1)} - \frac{\omega_j \omega_l (\nu_j + \nu_l)}{4g^2} \phi_j^{(1)} \phi_l^{(1)}\right]/A_j A_l, \quad \eta_{\mathrm{p}jl}^{+} = \mathrm{i}\omega^{+}\phi^{+}/gA_j A_l. \quad (4.5)$$

The difference-frequency expressions are similar and are not given here.

Given the hydrodynamic pressure, the wave forces and moments on a body can be obtained by direct integration over the instantaneous wetted body surface, $S(t)$:

$$(\boldsymbol{F}(t), \boldsymbol{M}(t)) = \iint_{S(t)} P(\boldsymbol{n}, \boldsymbol{r} \times \boldsymbol{n}) \, \mathrm{d}S. \quad (4.6)$$

Hereafter, we only give expressions for the forces; the corresponding expressions for moments can be obtained in a similar way. Using Taylor's expansion for both the pressure and unit normal vector of the instantaneous position $S(t)$ in (4.6) with respect to the body surface at rest (S_{B}), the integral over $S(t)$ can be transformed to a surface plus a waterline integral over the quiescent body position, S_{B} (details can be found in, for example, Ogilvie 1983). Upon collecting the contributions at each order, we can write the complete first- and second-order hydrodynamic forces as a sum of different components:

$$\boldsymbol{F}^{(1)} = \boldsymbol{F}_{\mathrm{R}}^{(1)} + \boldsymbol{F}_{\mathrm{I}}^{(1)} + \boldsymbol{F}_{\mathrm{D}}^{(1)} + \boldsymbol{F}_{\mathrm{HS}}^{(1)}, \quad (4.7)$$

$$\boldsymbol{F}^{(2)} = \boldsymbol{F}_{\mathrm{p}}^{(2)} + \boldsymbol{F}_{\mathrm{q}}^{(2)} + \boldsymbol{F}_{\mathrm{R}}^{(2)} + \boldsymbol{F}_{\mathrm{HS}}^{(2)} \quad (\boldsymbol{F}_{\mathrm{P}}^{(2)} = \boldsymbol{F}_{\mathrm{I}}^{(2)} + \boldsymbol{F}_{\mathrm{D}}^{(2)}), \quad (4.8)$$

where subscripts I, D and R represent respectively contributions from the incident, diffraction and radiation potentials, and HS the hydrostatic restoring forces. For the second-order force (4.8), $\boldsymbol{F}_{\mathrm{q}}^{(2)}$ represents the contribution from quadratic products of first-order quantities, and $\boldsymbol{F}_{\mathrm{p}}^{(2)}$ that due to directly to the second-order potential. The first-order components are given by:

$$\boldsymbol{F}_{\mathrm{R,I,D}}^{(1)} = -\rho_0 \iint_{S_{\mathrm{B}}} \frac{\partial \boldsymbol{\Phi}_{\mathrm{R,I,D}}^{(1)}}{\partial t} \boldsymbol{n} \, \mathrm{d}S, \quad (4.9)$$

$$\boldsymbol{F}_{\mathrm{HS}}^{(1)} = -\rho_0 g A_{\mathrm{w}} (\xi_z^{(1)} + y_{\mathrm{f}} \alpha_x^{(1)} - x_{\mathrm{f}} \alpha_y^{(1)}) \boldsymbol{k}, \quad (4.10)$$

where A_{w} is the waterplane area, $\boldsymbol{k}$ the unit vector in the z-direction, and x_{f} and y_{f} the locations of the longitudinal and transverse centres of floatation.

The second-order force components are given by

$$\boldsymbol{F}^{(2)}_{\mathrm{R,I,D}} = -\rho_0 \iint_{S_\mathrm{B}} \frac{\partial \boldsymbol{\Phi}^{(2)}_{\mathrm{R,I,D}}}{\partial t} \boldsymbol{n}\,\mathrm{d}S, \tag{4.11}$$

$$\boldsymbol{F}^{(2)}_{\mathrm{HS}} = -\rho_0 g A_\mathrm{w}(\xi^{(2)}_z + y_\mathrm{f}\alpha^{(2)}_x - x_\mathrm{f}\alpha^{(2)}_y)\boldsymbol{k}, \tag{4.12}$$

$$\begin{aligned}\boldsymbol{F}^{(2)}_\mathrm{q} = -\rho_0 \iint_{S_\mathrm{B}} &\left[\tfrac{1}{2}\nabla\boldsymbol{\Phi}^{(1)^2} + (\boldsymbol{\Xi}^{(1)} + \boldsymbol{\alpha}^{(1)} \times \boldsymbol{r})\cdot\frac{\partial}{\partial t}(\nabla\boldsymbol{\Phi}^{(1)})\right]\boldsymbol{n}\,\mathrm{d}S \\ &+ \tfrac{1}{2}\rho_0 g \int_\mathrm{WL} \zeta^{(1)^2}_\mathrm{r} N\,\mathrm{d}l + \boldsymbol{\alpha}^{(1)} \times \boldsymbol{F}^{(1)} \\ &- \rho_0 g A_\mathrm{w}\{\alpha^{(1)}_z(x_\mathrm{f}\alpha^{(1)}_x + y_\mathrm{f}\alpha^{(1)}_y)\}\boldsymbol{k},\end{aligned} \tag{4.13}$$

where $N = \boldsymbol{n}/(1-n_z^2)^{\frac{1}{2}}$, and for wall-sided bodies at the waterline, $N = \boldsymbol{n}$. In the above, the first-order relative wave height, $\zeta^{(1)}_\mathrm{r}$, is given by $\zeta^{(1)}_\mathrm{r} = \zeta^{(1)} - (\xi^{(1)}_z + y\alpha^{(1)}_x - x\alpha^{(1)}_y)$.

The first- and second-order motions follow from the equations of motions after collecting terms at the respective orders. For example, the translational modes in the absence of external forces are governed by

$$M_0 \frac{\partial^2}{\partial t^2}(\boldsymbol{\Xi}^{(1)} + \boldsymbol{\alpha}^{(1)} \times \boldsymbol{r}_\mathrm{G}) = \boldsymbol{F}^{(1)}, \tag{4.14}$$

$$M_0 \frac{\partial^2}{\partial t^2}(\boldsymbol{\Xi}^{(2)} + \boldsymbol{\alpha}^{(2)} \times \boldsymbol{r}_\mathrm{G}) = \boldsymbol{F}^{(2)} - M_0 \frac{\partial^2 \boldsymbol{H}}{\partial t^2}\boldsymbol{r}_\mathrm{G}, \tag{4.15}$$

where M_0 is the mass of the body, $\boldsymbol{r}_\mathrm{G}$ the position vector of the centre of gravity, and $\boldsymbol{F}^{(1)}$ and $\boldsymbol{F}^{(2)}$ are given by (4.7) and (4.8). As pointed out earlier, the second-order radiation problem for $\boldsymbol{\Phi}^{(2)}_\mathrm{R}$ is identical to that of the first-order radiation potential except for the change in frequencies, and the added mass and hydrodynamic damping coefficients for the second-order motions can be obtained similarly.

In the sequel, we focus on the second-order wave exciting forces which include all the nonlinear aspects. We define the second-order wave exciting forces as

$$\boldsymbol{F}^{(2)}_\mathrm{ex} = \boldsymbol{F}^{(2)}_\mathrm{I} + \boldsymbol{F}^{(2)}_\mathrm{D} + \boldsymbol{F}^{(2)}_\mathrm{q}. \tag{4.16}$$

In the presence of bichromatic waves, the second-order wave excitation (4.16) has the form

$$F^{(2)}_\mathrm{ex}(t) = \mathrm{Re}\sum_{j=1}^{2}\sum_{l=1}^{2}[A_j A_l f^{+}_{jl}\,\mathrm{e}^{-\mathrm{i}\omega^{+}t} + A_j A^{*}_l f^{-}_{jl}\,\mathrm{e}^{-\mathrm{i}\omega^{-}t}], \tag{4.17}$$

$$f^{\pm}_{jl} = f^{\pm}_{\mathrm{q}jl} + f^{\pm}_{\mathrm{p}jl}, \tag{4.18}$$

where $f^{\pm}$ are now the complete sum- and difference-frequency exciting force quadratic transfer functions (QTF's). For fixed bodies, for example (the more general case of freely floating or moored bodies can be readily derived from (4.11) and (4.13)) these force QTF's are given by

$$f^{+}_{\mathrm{q}jl} = \left[-\frac{\rho_0}{4}\iint_{S_\mathrm{B}}(\nabla\phi^{(1)}_j\cdot\nabla\phi^{(1)}_l)\boldsymbol{n}\,\mathrm{d}S - \frac{\rho_0\omega_j\omega_l}{4g}\int_\mathrm{WL}\phi^{(1)}_j\phi^{(1)}_l N\,\mathrm{d}l\right]/A_jA_l, \tag{4.19}$$

$$f^{-}_{\mathrm{q}jl} = \left[-\frac{\rho_0}{4}\iint_{S_\mathrm{B}}(\nabla\phi^{(1)}_j\cdot\nabla\phi^{(1)*}_l)\boldsymbol{n}\,\mathrm{d}S + \frac{\rho_0\omega_j\omega_l}{4g}\int_\mathrm{WL}\phi^{(1)}_j\phi^{(1)*}_l N\,\mathrm{d}l\right]/A_jA^{*}_l, \tag{4.20}$$

$$f_{\mathrm{p}jl}^{\pm} = \left[\rho_0 \mathrm{i}\omega^{\pm} \iint_{S_\mathrm{B}} (\phi_\mathrm{I}^{\pm} + \phi_\mathrm{D}^{\pm})\, \boldsymbol{n}\, \mathrm{d}S\right] / (A_j A_l, A_j A_l^*). \tag{4.21}$$

For later discussions, it is convenient to split f_p into its constituent components and write $f_\mathrm{p} = f_\mathrm{I} + f_\mathrm{B} + f_\mathrm{F}$, where f_I represents the second-order Froude–Krylov term, and f_B and f_F are contributions associated with the body and free-surface forcing terms, respectively.

For vertically axisymmetric bodies, the θ-integration in (4.19)–(4.21) can be performed independently. For example, the horizontal component of $f_{\mathrm{q}jl}^{+}$ in (4.19) has, upon integrating with respect to θ, the form

$$\begin{aligned} f_{x\mathrm{q}jl}^{+} = {} & \frac{\rho_0 g a n_\rho}{4(1-n_z^2)^{\frac{1}{2}}} \sum_{n=0}^{\infty} \frac{\pi}{\epsilon_n} (\psi_n^j \psi_{n+1}^l + \psi_n^l \psi_{n+1}^j)|_{z=0} + \frac{\rho_0 g^2}{4\omega_j \omega_l} \sum_{n=0}^{\infty} \int \rho n_\rho \, \mathrm{d}l \\ & \times \left[\frac{\pi}{\epsilon_n}\left(\frac{\partial \psi_n^j}{\partial \rho}\frac{\partial \psi_{n+1}^l}{\partial \rho} + \frac{\partial \psi_n^l}{\partial \rho}\frac{\partial \psi_{n+1}^j}{\partial \rho} + \frac{\partial \psi_n^j}{\partial z}\frac{\partial \psi_{n+1}^l}{\partial z} + \frac{\partial \psi_n^l}{\partial z}\frac{\partial \psi_{n+1}^j}{\partial z}\right)\right. \\ & \left. + \frac{\pi n(n+1)}{2\rho^2}(\psi_n^j \psi_{n+1}^l + \psi_n^l \psi_{n+1}^j)\right]. \end{aligned} \tag{4.22}$$

If only integrated quantities such as second-order forces are of interest, an indirect method (Molin 1979; Lighthill 1979), which does not require the solution for $\phi_\mathrm{D}^{\pm}$ explicitly, can be used as follows:

$$\iint_{S_\mathrm{B}} \phi_\mathrm{D}^{\pm} n_k \, \mathrm{d}S = \iint_{S_\mathrm{B}} \Psi_k^{\pm} \left(B^{\pm} - \frac{\partial \phi_\mathrm{I}^{\pm}}{\partial n}\right) \mathrm{d}S + \frac{1}{g} \iint_{S_\mathrm{F}} Q^{\pm} \Psi_k^{\pm} \, \mathrm{d}S, \tag{4.23}$$

where $\Psi_k^{\pm}$ are first-order assisting radiation potentials for mode k at the sum/difference frequency $\omega^{\pm}$, and satisfy the body boundary condition $\partial \Psi_k^{\pm}/\partial n = n_k$. For later reference in §5, we use the notation f_BB for the body integral that contains only $B^{\pm}$ in (4.23), and f_BI for the remaining body integral associated with ϕ_I^{-}.

In (4.23), the $B^{\pm}$ contain the second spatial derivatives of the first-order potential on the body, which are difficult to calculate with sufficient accuracy. To circumvent this problem, an alternative expression for $f_{\mathrm{BB}jl}^{\pm}$ corresponding to (2.23) can be derived using Stokes theorem to obtain finally

$$\begin{aligned} & \iint_{S_\mathrm{B}} \boldsymbol{n} \cdot [\Psi^{\pm} (\boldsymbol{\xi}_l^{(1)} \cdot \boldsymbol{\nabla}) \boldsymbol{\nabla} \phi_j^{\pm}] \, \mathrm{d}S \\ & \qquad = \int_\Gamma \Psi^{\pm} \, \mathrm{d}\boldsymbol{l} \cdot [\boldsymbol{\nabla} \phi_j^{(1)} \times \boldsymbol{\xi}_l^{(1)}] - \iint_{S_\mathrm{B}} \boldsymbol{n} \cdot [\boldsymbol{\nabla} \Psi^{\pm} \times (\boldsymbol{\nabla} \phi_j^{(1)} \times \boldsymbol{\xi}_l^{(1)})] \, \mathrm{d}S \end{aligned} \tag{4.24}$$

where Γ are all the boundaries of S_B.

For a uniform bottom-mounted vertical circular cylinder, the first-order diffraction and radiation potentials are available in closed forms. Using (4.23), semi-analytic expressions for the second-order forces and moments can also be derived. These are summarized in the Appendix. These expressions provide a useful benchmark for later second-order numerical results.

The present QTF's for bichromatic waves can be used to obtain predictions for the general case of a body interacting with a continuous spectrum of incident waves. The essential steps are outlined in §6.

5. Numerical results and discussion

The numerical procedure for solving the integral equation (3.3) follows essentially that in KY-I. The main steps are: (i) approximate the body contour, ∂_B, by N_p straight line segments; (ii) assume constant values for the potential $\phi^{\pm}_{Dn}$ over each segment; (iii) collocate the equations at the centre of each segment to obtain a system of linear algebraic equations for the segment unknowns; and (iv) solve the linear system for the unknown segment values. The numerical errors are essentially governed by the number of panels, N_p, and the number of circumferential Fourier modes, N, used in the general-order ring-source formulation.

As a first check of the present numerical method for bichromatic waves, we consider the special case of a single wave, $\omega_j = \omega_l$, and obtain identical results to the regular wave solutions of KY-I. We next check the convergence of the present second-order sum- and difference-frequency potential solutions with respect to the number of panels N_p, Fourier modes N, and partition radius b, for the free-surface integral evaluation. For these tests, we consider the diffraction of unidirectional bichromatic incident waves by a uniform (bottom-seated) vertical circular cylinder of radius a and depth $h = a$. In this case, semi-analytic results for the integrated forces can be derived (see Appendix) which provide a comparison for the present calculations. We select two typical frequency pairs $(\nu_j a, \nu_1 a) = (1, 2)$ and $(1.4, 1.6)$ respectively, which have the same mean (sum) frequency but frequency difference $\Delta\nu a = 1$ and 0.2 respectively.

Table 1 shows the convergence of the second-order potential horizontal force QTF's, $f^{\pm}_{pjl}$, with increasing number of panels, N_p, on the body. To follow the more rapid variations near the free-surface (especially for the sum-frequency potential), cosine-spaced segments (with smaller lengths near the free surface) are used. In this example, the maximum relative error is less than 0.3% when N_p is greater than 10. Owing to the smaller wavenumber associated with ϕ^- compared to that of ϕ^+, we obtain a faster convergence for f^-_{pjl}. In later numerical results, $N_p = 20$ segments are used for both first- and second-order calculations.

To show the convergence of the computed second-order sum- and difference-frequency potentials, $\phi^{\pm}$, with increasing numbers, $n \leqslant N$, of circumferential Fourier modes, the modal amplitudes of the potentials at $(\rho, z) = (a, 0)$ are given in table 2. The convergence of ϕ^+ with increasing number of modes is slower and less uniform than that of ϕ^-. This can be attributed to the slow convergence of Bessel functions with increasing orders for higher frequencies (arguments). This also indicates that there are greater variations in the circumferential direction of the sum-frequency wave run-up on the body as is seen later (see figures 6 and 7). The convergence rate of ϕ^- is faster for smaller frequency differences, while the convergence of ϕ^+ appears insensitive to changing difference frequencies. In the following calculations, $N = 9$ for the first-order problem (which is sufficient) and $N = 14$ and 9 respectively are used for the second-order sum- and difference-frequency problems.

The free-surface integral (3.12) is expensive to compute yet crucial to the overall accuracy. The method of §3 is used, and its convergence tested for varying partition radius, b. From John's (1950) expression of the free-surface Green function, we see that the decay rate of local waves is not sensitive to wave frequencies but depends primarily on the ratio ρ/h. Table 3 shows typical convergence of the sum- and difference-frequency second-order potential force QTF's, $f^{\pm}_{pjl}$, on a uniform vertical cylinder $(a/h = 1)$ with increasing b. Interestingly, the effects of local waves appear more localized for the difference-frequency problem. This was also pointed out by

	Difference frequency		Sum frequency	
$(\nu_j a, \nu_l a)$	(1.0, 2.0)	(1.4, 1.6)	(1.0, 2.0)	(1.4, 1.6)
Semi-analytic	1.936	0.435	2.656	2.875
$N_p = 10$	1.935	0.435	2.664	2.876
20	1.936	0.435	2.661	2.876
30	1.936	0.435	2.660	2.875

TABLE 1. Magnitudes of the second-order horizontal force QTF, $|f^{\pm}_{pjl}/\rho_0 g a A_j A_l|$, on a uniform vertical cylinder ($h/a = 1$) with increasing numbers of cosine-spaced segments, N_p, on the body. (A partition radius $(b-a)/h = 3$ is used for the free-surface integration.)

	Difference frequency		Sum frequency	
$(\nu_j a, \nu_l a) =$	(1.0, 2.0)	(1.4, 1.6)	(1.0, 2.0)	(1.4, 1.6)
$n = 0$	2.4178	12.5268	0.2368	0.2015
1	4.2202	4.1827	1.2925	1.3914
2	1.3129	0.2759	0.6589	0.7688
3	0.2763	0.0118	0.1915	0.0446
4	0.0361	0.0036	1.0461	1.0093
5	0.0169	0.0039	1.5603	1.4606
6	0.0016	0.0001	1.1920	1.1262
7	0.0010	0.0001	0.4556	0.4683
8	0.0001	*	0.0969	0.1027
9	*	*	0.0168	0.0177
10	*	*	0.0023	0.0026
11	*	*	0.0002	0.0003
12	*	*	*	*
13	*	*	*	*
14	*	*	*	*

TABLE 2. Convergence of the sum- and difference-frequency potential modal amplitudes $|\phi^{\pm}_n/(gA_j A_l/2a(\omega_j \omega_l)^{\frac{1}{2}})|$ on the waterline ($\rho = a$ and $z = 0$) of a uniform vertical cylinder ($h/a = 1$). (* indicate values less than 0.0001.)

Kagemoto & Yue (1986) in the study of multiple-body interactions including evanescent waves. From table 3, it is seen that a partition radius of $(b-a) \sim 3h$ is sufficient for 3 significant decimals of accuracy, and this value is used in all later computations. The excellent accuracy with relatively small inner numerical integration domains again underscores the efficacy of the present free-surface integral method.

Having demonstrated the convergence of the present numerical method through comparisons to semi-analytic solutions, we now present complete second-order QTF results for several typical geometries: a uniform (bottom-mounted) vertical circular cylinder of depth-to-radius ratio $h/a = 1$ and 4; a fixed hemisphere; and a freely floating hemisphere. One of the objectives is to compare the complete (in the context of second-order diffraction theory) QTF's with a number of popular approximation methods for predicting sum- and difference-frequency wave excitations and

	Difference frequency		Sum frequency	
$(\nu_j a, \nu_i a) =$	(1.0, 2.0)	(1.4, 1.6)	(1.0, 2.0)	(1.4, 1.6)
Semi-analytic	1.936	0.435	2.656	2.875
$(b-a)/h = 2$	1.936	0.435	2.668	2.861
3	1.936	0.435	2.661	2.876
4	1.936	0.435	2.659	2.877

TABLE 3. Magnitudes of the second-order sum- and difference-frequency potential force QTF's, $|f^{\pm}_{pji}/\rho_0 g a A_j A_i|$, on a uniform vertical circular cylinder ($h/a = 1$). The results for different partition radii b are compared to semi-analytic solutions (Appendix). ($N_p = 20$ is used on the body.)

responses. These approximations are typically based on heuristic arguments and neglect one or more of the second-order components. The validity and usefulness of the different methods, which depend on the frequency combinations, body geometry and water depths, have so far not been established (e.g. Ogilvie 1983) primarily because complete second-order results have not been readily available. In addition to force and moment QTF's, the QTF's of local quantities such as pressure and wave run-up are also presented, revealing a number of interesting behaviours. For ease of presentation, the following results are organized separately for the sum- and difference-frequency problems.

5.1. *The difference-frequency problem*

Existing approximations for this problem are usually based on the assumption that the incident irregular waves are narrow-banded so that difference-frequency wave excitations are *slowly varying*. One approach, due to Newman (1974), is to replace the total QTF by the mean drift force operator f^-_{qjj}. Marthinsen (1983) suggested a similar approximation based upon a slowly varying wave envelope (Hilbert transform) idea wherein the mean drift force operator of the instantaneous local frequency is used instead. These methods greatly simplify the problem since the mean drift forces can be computed from the first-order potential only. As a result, they have been widely used in practical applications although the restrictions on narrow-bandedness and small gradients (with respect to frequency difference) of the QTF on the monochromatic diagonal have not been quantified. Improvements on these approximations typically include one or more of the missing second-order contributions, usually based on the fact that they can be fairly readily obtained. Examples include the incomplete QTF operators $(f^-_q + f^-_I)$ of Standing & Dacunha (1982); and $f^- \approx f^-_q + f^-_I + f^-_{BI}$ used by Pinkster (1980). All such approximations exclude the more difficult contributions due to second-order forcing on the body by first-order motions, f^-_{BB}, and that due to the free-surface inhomogeneous terms, f^-_F.

In table 4, the complete second-order difference-frequency horizontal force QTF together with its constituent components are given for a bottom-mounted uniform vertical cylinder ($h/a = 1$ and 4) for different incident frequency combinations. The qualitative trends are similar for the two depths although the force magnitudes are smaller for the deeper cylinder. For a fixed sum frequency and increasing frequency difference, $\Delta\nu a$, the contributions from the second-order potential, f^-_I, f^-_B, and f^-_F, increase almost linearly starting from zero on the diagonal; while the linear quadratic term f^-_q remains more or less the same. As a result, f^-_q dominates the other

$\nu_i a$		$\nu_j a$ = 1.0	1.2	1.4	1.6	1.8	2.0
1.0	0.666	0.918	0.864	0.811	0.765	0.722	0.680
	0	0	0.297	0.550	0.770	0.963	1.131
	0	0	0.302	0.568	0.794	0.966	1.063
	0	0	0.037	0.097	0.166	0.229	0.273
	0.666	0.918	0.982	1.163	1.347	1.489	1.575
1.2	0.647	0.636	0.826	0.791	0.758	0.723	0.685
	0.168	0	0	0.255	0.481	0.683	0.864
	0.167	0	0	0.259	0.493	0.697	0.854
	0.034	0	0	0.036	0.097	0.166	0.226
	0.689	0.636	0.826	0.870	1.011	1.165	1.294
1.4	0.612	0.612	0.603	0.772	0.753	0.729	0.698
	0.337	0.166	0	0	0.229	0.437	0.626
	0.331	0.165	0	0	0.231	0.445	0.632
	0.088	0.034	0	0	0.036	0.099	0.166
	0.763	0.640	0.603	0.772	0.810	0.925	1.054
1.6	0.578	0.588	0.594	0.600	0.748	0.735	0.712
	0.504	0.332	0.164	0	0	0.211	0.406
	0.481	0.325	0.164	0	0	0.213	0.411
	0.150	0.093	0.035	0	0	0.037	0.101
	0.856	0.701	0.615	0.600	0.748	0.777	0.867
1.8	0.552	0.567	0.583	0.602	0.615	0.732	0.717
	0.664	0.497	0.329	0.163	0	0	0.198
	0.602	0.471	0.322	0.163	0	0	0.200
	0.208	0.158	0.096	0.037	0	0	0.038
	0.943	0.788	0.678	0.619	0.615	0.732	0.749
2.0	0.534	0.547	0.566	0.593	0.615	0.624	0.711
	0.809	0.653	0.491	0.327	0.163	0	0
	0.676	0.586	0.463	0.319	0.162	0	0
	0.243	0.215	0.161	0.099	0.038	0	0
	1.009	0.877	0.765	0.678	0.629	0.624	0.711
	$\nu_j a$ =	1.0	1.2	1.4	1.6	1.8	2.0

TABLE 4. Magnitudes of the components of the second-order difference-frequency horizontal force QTF, $|f_{ji}^-/\rho_0 g a A_j A_i^*|$, on a uniform vertical cylinder. The upper right triangular matrix is for $h/a = 1$, and lower half for $h/a = 4$. Each element satisfies the symmetry relation $f_{ji}^- = f_{ij}^{-*}$. Computed values are for: first row, $|f_{Gji}^-|$; second row, $|f_{Iji}^-|$; third row, $|f_{Bji}^-|$; fourth row, $|f_{Fji}^-|$; and fifth row, the complete QTF $|f_{ji}^-|$.

contributions near the diagonal, while for larger frequency differences, the contributions due to the second-order incident waves, f_I^- and f_B^-, dominate. The computationally difficult free-surface contribution term, f_F^-, remains small overall.

The relatively rapid growth of f_I^- and f_B^- with increasing $\Delta\nu a$ indicates that the validity of Newman's (1974) or Marthinsen's (1983) approximations is quite sensitive to the narrow-bandedness of the input spectrum. On the other hand, Pinkster's (1980) approximation (or QIB approximation†) which excludes only f_F^- is expected to give acceptable results for a broader range of frequency combinations without

† Pinkster (1980) used only an approximated f_{BI}^- for the body-forcing contribution even for freely floating bodies. In this sense, we call the more general approximation that also includes f_{BB}^- in the body-forcing contribution the 'QIB' approximation method.

$\nu_j a =$		1.0	1.2	1.4	1.6	1.8	2.0
$\nu_i a$	0.173	0.003	0.063	0.115	0.155	0.185	0.207
1.0	0	0	0.148	0.272	0.377	0.464	0.533
	0	0	0.018	0.048	0.080	0.110	0.130
	0.173	0.003	0.345	0.624	0.848	1.016	1.126
	0.203	0.173	0.044	0.080	0.120	0.154	0.182
1.2	0.318	0	0	0.127	0.238	0.334	0.415
	0.055	0	0	0.017	0.047	0.080	0.108
	0.729	0.173	0.044	0.303	0.548	0.750	0.908
	0.257	0.196	0.178	0.076	0.099	0.128	0.157
1.4	0.559	0.315	0	0	0.114	0.216	0.306
	0.130	0.055	0	0	0.018	0.048	0.080
	1.232	0.708	0.178	0.076	0.281	0.500	0.687
	0.299	0.235	0.194	0.181	0.096	0.111	0.134
1.6	0.702	0.552	0.312	0	0	0.105	0.201
	0.197	0.133	0.056	0	0	0.018	0.049
	1.539	1.184	0.690	0.181	0.096	0.267	0.469
	0.321	0.264	0.218	0.188	0.176	0.106	0.117
1.8	0.766	0.691	0.546	0.310	0	0	0.099
	0.249	0.207	0.138	0.058	0	0	0.018
	1.682	1.465	1.144	0.673	0.176	0.106	0.259
	0.325	0.282	0.240	0.205	0.178	0.165	0.112
2.0	0.782	0.753	0.683	0.542	0.309	0	0
	0.268	0.258	0.211	0.143	0.060	0	0
	1.717	1.597	1.412	1.113	0.661	0.165	0.112
$\nu_j a =$	1.0	1.2	1.4	1.6	1.8	2.0	

TABLE 5. Magnitudes of the components of the second-order difference-frequency pitch moment QTF, $|M_{ji}^-/\rho_0 g a^2 A_j A_i^*|$, on a uniform vertical cylinder. The upper right triangular matrix is for $h/a = 1$, and lower half for $h/a = 4$. Each element satisfies the symmetry relation $M_{ji}^- = M_{ij}^{-*}$. Computed values are for: first row, $|M_{\mathrm{q}ji}^-|$; second row, $|M_{\mathrm{I}ji}^-|$; third row, $|M_{\mathrm{F}ji}^-|$; and fourth row, the complete QTF $|M_{ji}^-|$.

considerable increase of computation time. This was also observed by Eatock Taylor *et al.* (1988).

Table 5 shows the difference-frequency pitch moment (with respect to the waterplane centre) QTF's on a uniform vertical cylinder, $h/a = 1$ and 4. The behaviour of the body-surface forcing contribution M_{B}^- here is very similar to M_{I}^- (see also table 4) and is not given separately. Unlike the horizontal force, the moment QTF's are greater for the deeper cylinder, and the components associated with ϕ_{I}^-, M_{I}^- and M_{B}^-, dominate M_{q}^- in most of the cases. This can be attributed to the slow depth attenuation of ϕ_{I}^- for small $\Delta\nu a$ (see (2.7)), which results in a lower centre of pressure and a larger moment arm. To show this feature more clearly, we present in figure 1 the second-order potential pressure QTF's, p_{p}^-, as compared to the first-order quadratic pressure QTF's, p_{q}^-, on the side of the $h/a = 4$ cylinder for two incident frequency combinations, $(\nu_j a, \nu_i a) = (1, 2)$ and $(1.4, 1.6)$. The behaviour of the second-order potential pressure, p_{p}^-, is dominated by ϕ_{I}^- and its diffracted free wave, with a depth attenuation rate characterized by the wavenumber $k_j - k_i$ or k_2^-. Thus, for smaller $\Delta\nu a$, p_{p}^- becomes comparably small in magnitude but penetrates deeper on all sides of the cylinder. In this case, ϕ_{I}^- behaves like long waves in shallow water,

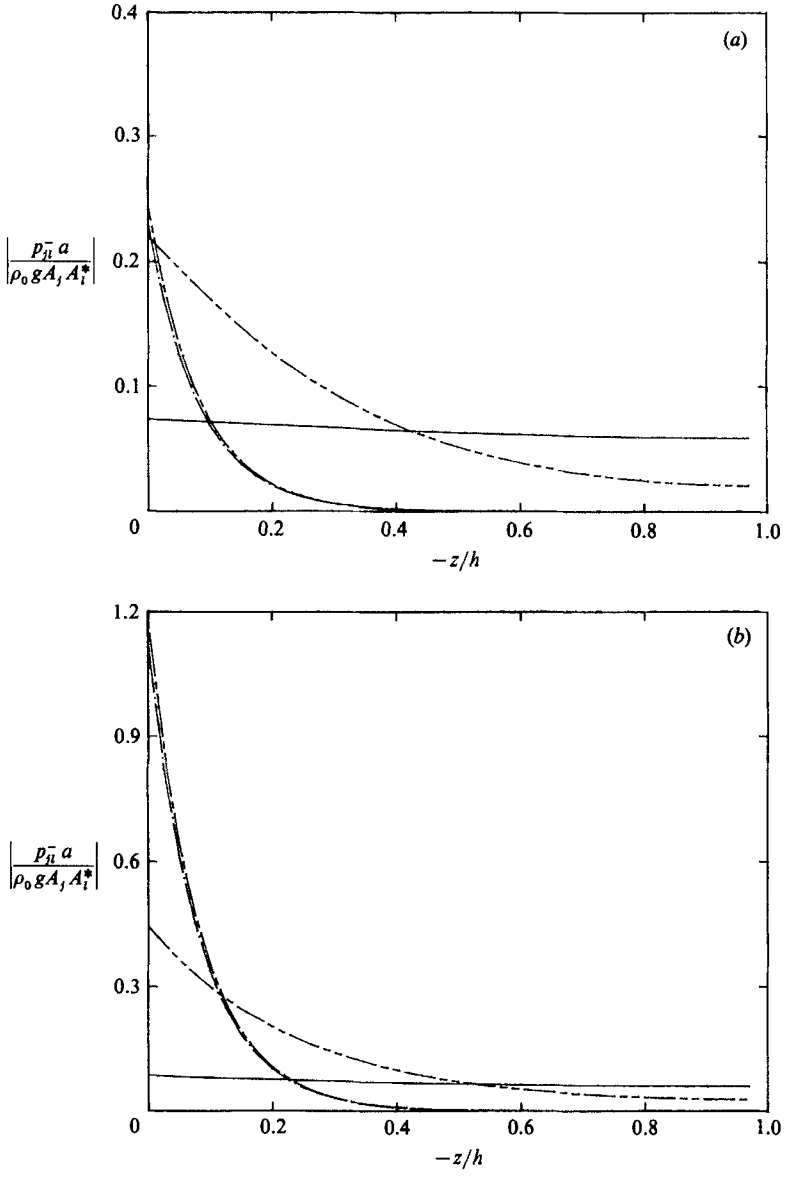

FIGURE 1. The second-order difference-frequency pressure QTF on the side of a uniform vertical cylinder, radius a, depth $h = 4a$. The curves are for: $|p_{qjl}^-|$ for $\nu_j a, \nu_l a = 1, 2$ (—·—); 1.4, 1.6 (– – –); and $|p_{pjl}^-|$ for $\nu_j a, \nu_l a = 1, 2$ (– – – –); 1.4, 1.6 (——). (*a*) lee side ($\theta = 0$); and (*b*) weather side ($\theta = \pi$).

and the associated pressures are almost uniform to the bottom. These deeply penetrating local pressures contribute significantly to the pitch moment through increased moment arms. In conrast, the quadratic pressure p_q^- attenuates rapidly according to the wavenumber $k_j + k_l$, and does not contribute appreciably to the pitch moment. It is interesting to note that the magnitudes of M_F^- are also appreciably increased near the diagonal owing to the slow depth attenuation of the locked waves on the *lee side* as can be expected from (2.31).

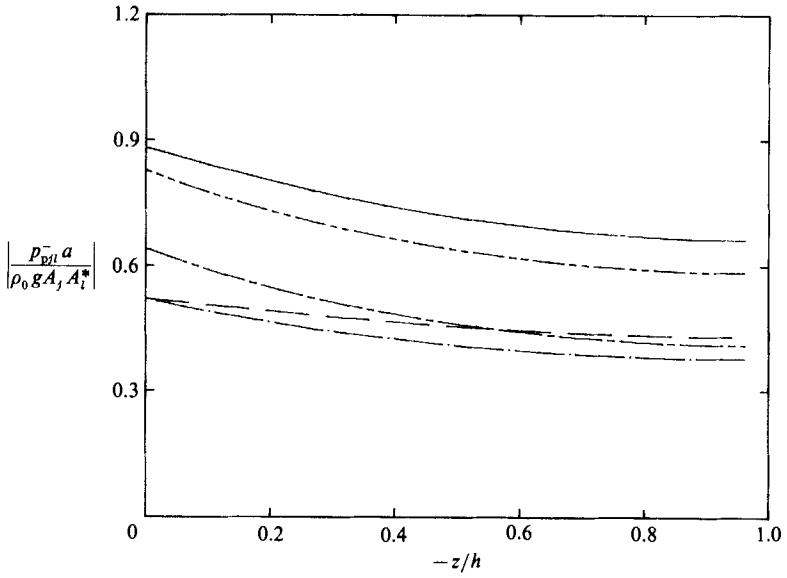

FIGURE 2. The second-order difference-frequency potential pressure QTF, $|p_{pjl}^{-}|$, on a uniform vertical cylinder ($h/a = 1$), for $(\nu_j a, \nu_l a) = (1, 2)$, and at angular positions: $\theta = 0$ (------), $\frac{1}{4}\pi$ (—·—), $\frac{1}{2}\pi$ (— — —), $\frac{3}{4}\pi$ (— — — —), and π (——).

In view of these effects associated with the behaviour of the second-order incident and free waves, the validity of Newman's (1974), Marthinsen's (1983), and Standing & Dacunha's (1982) approximations may be limited, especially for pitch-roll excitations of deep-draught bodies. These results indicate that the components associated with ϕ_{I}^{-} are important for the prediction of slowly varying pitch moments on deep-draught platforms, particularly when the centre of rotation is located close to the free surface.

To further illuminate the local behaviour of the second-order difference-frequency potential, we plot in figure 2 its associated pressure QTF, p_{p}^{-}, as a function of depth at five angular positions on the vertical cylinder, $h/a = 1$, and incident frequencies $(\nu_j a, \nu_l a) = (1, 2)$. Because of the dominant contribution from ϕ_{I}^{-}, the variation of p_{p}^{-} along the circumference is quite small in contrast to the sum-frequency case (see figure 5). The effect of the angular-dependent free-surface forcing term is not appreciable in this figure. In figure 3, we show the run-up QTF, η_{p}^{-}, associated with the second-order potential on the $h/a = 1$ cylinder. For comparison, the run-up QTF, η_{q}^{-}, due to quadratic products of first-order potentials is also plotted. The angular variation of η_{p}^{-} is much milder than that of η_{q}^{-}, as can be expected from the behaviour of ϕ_{I}^{-}. In particular, for small $\Delta\nu a$, η_{p}^{-} is almost a constant on the cylinder.

We next consider the difference-frequency wave excitations on alternatively a fixed and a freely floating hemisphere of radius a in depth $h = 3a$. In this case, the first-order solutions for wave exciting forces, added mass, hydrodynamic damping, and motions are first checked and confirmed against the results obtained, for example, by Hulme (1982) and Pinkster (1980). Table 6 shows the complete difference-frequency horizontal and vertical force QTF's as well as their constituent components for a fixed hemisphere. Comparing with the QTF's for the cylinder (table 4), here f_{q}^{-} (especially for the horizontal force) is the most important contribution in

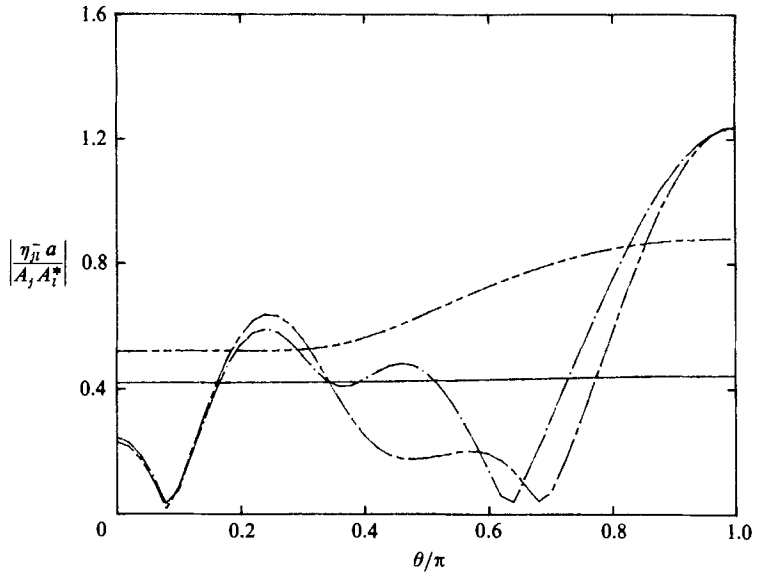

FIGURE 3. The second-order difference-frequency run-up QTF's, η_{jl}^- and η_{pjl}^-, on a uniform vertical cylinder ($h/a = 1$). The curves are: $|\eta_{qjl}^-|$ for $\nu_j a, \nu_l a = 1, 2$ (—·—); 1.4, 1.6 (— — —); and $|\eta_{pjl}^-|$ for $\nu_j a, \nu_l a = 1, 2$ (— — — —); 1.4, 1.6 (——).

almost all frequency combinations. The components f_{I}^- and f_{BI}^- also contribute appreciably, while the free-surface component remains small. The second-order potential force QTF, f_{p}^-, has in general milder/faster variations compared to f_{q}^- with increasing frequency sums/differences. The components of the vertical force, f_{q}^- and $(f_{\mathrm{I}}^- + f_{\mathrm{B}}^-)$, are in general in phase so that the complete QTF f_{jl}^- is always larger than the individual components. The opposite trend is seen for the horizontal forces. Consequently, the gradient (with respect to $\Delta\nu$) of the vertical force QTF near the diagonal is steeper than that of the horizontal force QTF. The mean vertical drift force, which is given on the diagonal, is *negative* and is comparable in magnitude with the horizontal mean drift force.

Similar results for the freely floating hemisphere are given in table 7. As pointed out earlier, we separate the contributions due to the body forcing into two parts, f_{BI}^- and f_{BB}^-, where f_{BI}^- represents the diffraction effect of ϕ_{I}^-, and f_{BB}^- the contribution associated with first-order motions, in this case (and for table 12) calculated using the more robust (4.24). The result for the component, $f_{\mathrm{I}}^- + f_{\mathrm{BI}}^-$, is identical to that in table 6 and not repeated here. In general, the trends for the relative magnitudes of the individual contributions are similar to that of table 6. As expected, the effect of first-order motions in f_{q}^- and f_{F}^- decreases with increasing sum frequencies. The contribution of the body forcing due to first-order motions, f_{BB}^-, as well as the free-surface contribution, f_{F}^-, are found to be less important compared to the other terms, especially near the diagonal. However, because of the possible phase cancellations among the contributions, neglecting f_{F}^- or f_{BB}^- for certain cases may not be acceptable particularly for large $\Delta\nu a$. For example, for $(\nu_j a, \nu_l a) = (1, 2)$ in table 7, the component from the free-surface integral is 70% of the total horizontal force QTF. As will be shown later (see tables 11 and 12), this first-order motion effect is much more significant in the sum-frequency problem. The mean drift forces for a freely floating (or fixed) hemisphere given by the diagonal terms in table 7 (or table 6) are

$\nu_j a =$		0.8	1.0	1.2	1.4	1.6	1.8	2.0
$\nu_i a$								
0.8	0.510	0.375	0.427	0.454	0.461	0.461	0.461	0.462
	0	0	0.063	0.144	0.253	0.381	0.513	0.627
	0	0	0.015	0.039	0.071	0.105	0.137	0.156
	0.510	0.375	0.416	0.418	0.389	0.346	0.302	0.267
1.0	0.484	0.538	0.471	0.493	0.498	0.497	0.495	0.494
	0.298	0	0	0.061	0.140	0.246	0.369	0.495
	0.010	0	0	0.014	0.038	0.070	0.104	0.132
	0.792	0.538	0.471	0.482	0.459	0.415	0.360	0.304
1.2	0.445	0.512	0.499	0.513	0.517	0.516	0.515	0.513
	0.274	0.280	0	0	0.060	0.138	0.241	0.362
	0.036	0.011	0	0	0.013	0.038	0.069	0.102
	0.749	0.803	0.499	0.513	0.505	0.472	0.422	0.362
1.4	0.402	0.478	0.477	0.468	0.523	0.525	0.526	0.525
	0.248	0.258	0.272	0	0	0.059	0.136	0.238
	0.076	0.040	0.012	0	0	0.013	0.037	0.069
	0.702	0.770	0.760	0.468	0.523	0.511	0.478	0.428
1.6	0.358	0.440	0.449	0.450	0.442	0.531	0.536	0.538
	0.227	0.232	0.250	0.267	0	0	0.059	0.135
	0.128	0.082	0.042	0.013	0	0	0.012	0.037
	0.647	0.731	0.734	0.728	0.442	0.531	0.522	0.489
1.8	0.315	0.398	0.414	0.424	0.425	0.417	0.545	0.551
	0.238	0.211	0.222	0.245	0.264	0	0	0.058
	0.191	0.137	0.087	0.044	0.013	0	0	0.012
	0.583	0.681	0.701	0.706	0.701	0.417	0.545	0.536
2.0	0.274	0.356	0.376	0.392	0.401	0.401	0.392	0.560
	0.300	0.225	0.201	0.215	0.241	0.262	0	0
	0.263	0.203	0.144	0.090	0.045	0.013	0	0
	0.516	0.621	0.655	0.676	0.681	0.675	0.392	0.560
$\nu a =$	0.8	1.0	1.2	1.4	1.6	1.8	2.0	

TABLE 6. Magnitudes of the components of the second-order difference-frequency force QTF, $|f_{ji}^{-}/\rho_0 g a A_j A_i^*|$, on a fixed hemisphere ($h/a = 3$). The upper right triangular matrix is for the horizontal force, and the lower half the vertical force. Each element satisfies the symmetry relation, $f_{ji}^{-} = f_{ij}^{-*}$. Computed values are for: first row, $|f_{Qji}^{-}|$; second row, $|f_{Iji}^{-} + f_{Bji}^{-}|$; third row, $|f_{Bji}^{-}|$; and fourth row, the complete QTF $|f_{ji}^{-}|$.

in good agreement with the results of Pinkster (1980) and Molin (1983). Note that the mean vertical force in table 7 changes sign in the vicinity of the heave reasonance frequency, $\nu a \sim 1$.

We finally present results for the second-order heave and surge motions of the freely floating hemisphere at the difference frequency of the incoming bichromatic waves. These can be obtained from (4.15) in terms of the exciting force QTF's, f_{ji}^{-}. It is interesting to note that the second-order heave and surge motions are mutually independent but are both coupled to the first-order surge and heave motions through the body boundary forcing term, B. For any pair of bichromatic waves whose frequency sum or difference coincide with the natural frequency of a particular mode, second-order resonance can occur. This is seen in table 8 for the difference-frequency response QTF's where a heave resonance is observed for the wave pair, $(\nu_j a, \nu_i a) = (1, 4)$. Because of the large hydrodynamic damping near the heave resonance

$\nu_j a =$		0.8	1.0	1.2	1.4	1.6	1.8	2.0
$\nu_i a$	0.669	0.071	0.398	0.522	0.411	0.359	0.352	0.358
0.8	0	0	0.018	0.053	0.072	0.091	0.115	0.147
	0	0	0.038	0.062	0.103	0.158	0.215	0.269
	0.669	0.071	0.372	0.475	0.351	0.266	0.217	0.196
	0.568	0.306	0.519	0.719	0.619	0.534	0.482	0.447
1.0	0.032	0	0	0.015	0.026	0.040	0.060	0.084
	0.025	0	0	0.028	0.072	0.129	0.189	0.247
	0.270	0.306	0.519	0.709	0.591	0.483	0.407	0.354
	0.135	0.189	0.494	0.878	0.783	0.718	0.681	0.653
1.2	0.081	0.030	0	0	0.004	0.010	0.020	0.036
	0.046	0.023	0	0	0.020	0.060	0.109	0.160
	0.213	0.469	0.494	0.878	0.766	0.660	0.570	0.487
	0.121	0.376	0.526	0.488	0.717	0.677	0.660	0.648
1.4	0.107	0.063	0.018	0	0	0.005	0.010	0.019
	0.042	0.039	0.015	0	0	0.015	0.047	0.087
	0.320	0.630	0.817	0.488	0.717	0.658	0.598	0.529
	0.204	0.430	0.516	0.457	0.426	0.652	0.645	0.639
1.6	0.130	0.090	0.040	0.014	0	0	0.003	0.008
	0.065	0.061	0.040	0.012	0	0	0.013	0.042
	0.369	0.681	0.820	0.742	0.426	0.652	0.627	0.581
	0.241	0.447	0.499	0.434	0.407	0.392	0.644	0.643
1.8	0.154	0.113	0.060	0.028	0.012	0	0	0.002
	0.111	0.098	0.077	0.039	0.011	0	0	0.013
	0.387	0.694	0.813	0.730	0.686	0.392	0.644	0.626
	0.259	0.448	0.476	0.409	0.386	0.378	0.370	0.646
2.0	0.177	0.134	0.077	0.043	0.023	0.010	0	0
	0.171	0.150	0.126	0.080	0.041	0.012	0	0
	0.383	0.680	0.788	0.713	0.676	0.655	0.370	0.646
$\nu_a =$	0.8	1.0	1.2	1.4	1.6	1.8	2.0	

TABLE 7. Magnitudes of the components of the second-order difference-frequency force QTF, $|f_{ji}^-/\rho_0 g a A_j A_i^*|$, on a freely floating hemisphere ($h/a = 3$). The upper right triangular matrix is for the horizontal force, and the lower half the vertical force. Each element satisfies the symmetry relation, $f_{ji}^- = f_{ij}^{-*}$. Computed values are for: first row, $|f_{\mathrm{Q}ji}^-|$; second row, $|f_{\mathrm{BB}ji}^-|$; third row, $|f_{\mathrm{F}ji}^-|$; and fourth row, the complete QTF $|f_{ji}^-|$.

$\nu_j a =$	0.6	1.0	1.4
$\nu_i a$	0.161 (0.175)	0.378 (0.188)	0.366 (0.133)
3.6	0.207 (0.049)	0.455 (0.067)	0.240 (0.075)
4.0	0.150 (0.230)	0.373 (0.170)	0.338 (0.103)
	0.112 (0.051)	0.684 (0.050)	0.298 (0.044)
4.4	0.144 (0.205)	0.333 (0.219)	0.300 (0.029)
	0.071 (0.041)	0.495 (0.056)	0.390 (0.010)

TABLE 8. Second-order difference-frequency heave and surge response QTF's, $|\xi_{ji}^- a/A_j A_i^*|$, for a freely-floating hemisphere ($h/a = 3$). The results are for: first row, the complete exciting force QTF; and second row, the complete response QTF. The surge exciting force and response QTF's are given in parentheses.

$\nu_j a =$		1.0	1.2	1.4	1.6	1.8	2.0
$\nu_i a$							
1.0	1.493	1.440	1.577	1.709	1.802	1.828	1.778
	3.004	1.636	1.963	2.308	2.582	2.710	2.661
	1.518	0.939	0.782	0.778	0.850	0.903	0.886
1.2	1.546	1.641	1.676	1.764	1.813	1.797	1.709
	3.179	3.723	2.262	2.549	2.752	2.807	2.682
	1.641	2.084	0.752	0.847	0.959	1.013	0.973
1.4	1.681	1.774	1.868	1.805	1.808	1.753	1.634
	3.408	4.035	4.472	2.754	2.876	2.857	2.671
	1.748	2.262	2.612	0.971	1.074	1.105	1.037
1.6	1.850	1.909	1.945	1.957	1.772	1.689	1.556
	3.685	4.211	4.654	4.975	2.930	2.872	2.668
	1.853	2.302	2.714	3.021	1.160	1.184	1.114
1.8	1.969	1.981	1.957	1.910	1.820	1.593	1.467
	3.769	4.162	4.454	4.843	5.097	2.816	2.688
	1.809	2.182	2.505	2.935	3.277	1.226	1.227
2.0	1.995	1.959	1.878	1.786	1.677	1.544	1.368
	3.613	3.852	3.961	4.159	4.695	5.043	2.693
	1.620	1.899	2.094	2.375	3.018	3.052	1.334
$\nu_j a =$	1.0	1.2	1.4	1.6	1.8	2.0	

TABLE 9. Magnitudes of the components of the second-order sum-frequency horizontal force QTF, $|f_{jl}^{+}/\rho_0 g a A_j A_l|$, on a uniform vertical cylinder. The upper right triangular matrix is for $h/a = 1$, and lower half for $h/a = 4$. Each element satisfies the symmetry relation $f_{jl}^{+} = f_{lj}^{+}$. Computed values are for: first row, $|f_{qjl}^{+}|$; second row, $|f_{pjl}^{+}|$; and third row total QTF, $|f_{jl}^{+}| = |f_{qjl}^{+} + f_{pjl}^{+}|$.

frequency at $\nu a \sim 1$, the resonance amplitude is small and gives only about 1% correction to the first-order motion amplitude at that frequency for wave steepnesses of the order $(kA)_{j,l} \sim 0.1$. In this frequency range, the surge response QTF is typically only about 10% of that in heave, although the horizontal and vertical force QTF's are of the same order of magnitude.

5.2. *The sum-frequency problem*

Unlike the difference-frequency problem, where the zero difference-frequency (mean) force can be obtained directly from first-order potentials only, the sum-frequency force QTF's cannot be likewise estimated even in the case of a single regular wave. For this reason, relatively few useful studies have been made for the sum-frequency problem. One attempt is that of Herfjord & Nielsen (1986) who applied the linear quadratic operator, f_{q}^{+}, in place of the complete QTF, f_{jl}^{+}. This was also used by Petrauskas & Liu (1987) in estimating the loads of the tendons of a tension-leg platform. This was found to *underestimate* the experimental measurements by as much as a factor of 3 or 4. Another idea is that of De Boom *et al.* (1983) who included also the terms associated with the second-order incident potential $(f_{\mathrm{q}}^{+} + f_{\mathrm{I}}^{+} + f_{\mathrm{BI}}^{+})$, somewhat analogous to Pinkster's (1980) approach for the difference-frequency problem. Again, the more difficult terms such as f_{BB}^{+} and f_{F}^{+} are ignored in these approximations. Unlike the difference-frequency case, there is little basis for justifying such approximations regardless of whether the incident waves are narrow-banded or not.

In table 9, we present the sum-frequency horizontal force QTF's on the bottom-

$\nu_i a$		$\nu_j a$ = 1.0	1.2	1.4	1.6	1.8	2.0
1.0	0.235	0.217	0.199	0.184	0.166	0.145	0.121
	4.472	0.785	0.942	1.089	1.194	1.228	1.179
	4.309	0.635	0.794	0.939	1.048	1.094	1.063
1.2	0.254	0.262	0.181	0.164	0.147	0.126	0.103
	4.220	4.934	1.071	1.181	1.252	1.256	1.180
	4.028	4.738	0.927	1.039	1.117	1.136	1.079
1.4	0.272	0.267	0.259	0.147	0.130	0.109	0.086
	3.762	4.777	5.237	1.251	1.285	1.262	1.167
	3.524	4.554	5.011	1.116	1.162	1.156	1.082
1.6	0.279	0.264	0.245	0.223	0.112	0.094	0.073
	3.481	4.333	5.079	5.580	1.295	1.265	1.179
	3.219	4.092	4.851	5.364	1.185	1.173	1.106
1.8	0.270	0.248	0.223	0.196	0.168	0.078	0.063
	3.088	3.739	4.332	5.231	6.037	1.255	1.217
	2.829	3.505	4.120	5.037	5.869	1.178	1.155
2.0	0.246	0.221	0.191	0.164	0.138	0.116	0.058
	2.569	3.008	3.351	3.983	5.421	6.502	1.254
	2.331	2.798	3.168	3.821	5.283	6.387	1.198
$\nu_j a$ =	1.0	1.2	1.4	1.6	1.8	2.0	

TABLE 10. Magnitudes of the components of the second-order sum-frequency pitch moment QTF, $|M^+_{jl}/\rho_0 g a^2 A_j A_l|$, on a uniform vertical cylinder. The upper right triangular matrix is for $h/a = 1$, and lower half for $h/a = 4$. Each element satisfies the symmetry relation $M^+_{jl} = M^+_{lj}$. Computed values are for: first row, $|M^+_{qjl}|$; second row, $|M^+_{pjl}|$; and third row total QTF, $|M^+_{qjl} + M^+_{pjl}|$.

mounted vertical cylinder of depths $h/a = 1$ and 4 for different incident frequency combinations. Unlike the difference-frequency problem, the components associated with the second-order incident wave, f^+_{I} and f^+_{BI}, are almost negligible in the frequency range considered and are hence omitted. (However, we remark that these contributions may be important for small kh, as can be seen from (2.6).) In this case, most of the second-order potential contribution f^+_{p} comes from the free-surface integral term f^+_{F}. The force, f^+_{F}, is in general greater than f^+_{q} and becomes more important for the deeper cylinder. For a fixed frequency difference and increasing sum frequencies, f^+_{p} oscillates in magnitude but increases rapidly, which accounts for the relative importance of the sum-frequency potential contribution for higher sum frequencies. On the other hand, for fixed sum frequency and increasing frequency differences, f^+_{p} decreases rapidly (especially for the $h/a = 4$ case). These features are mainly due to the behaviour of the second-order potential pressure suggested by the far-field asymptotic form (2.31), as will be explained later. Note that f^+_{q} and f^+_{p} are generally out of phase, so that the total force QTF's are typically smaller.

Similar results for the sum-frequency pitch moment QTF's with respect to the waterplane centre are given in table 10. In this case, M^+_{p} is generally much greater than M^+_{q} especially for the deeper cylinder. This can be attributed to the deep penetration of the sum-frequency second-order diffraction potential, ϕ^+_{D}, or more precisely the particular solution, ϕ^+_{p}. To show this, we plot in figure 4 the sum-frequency pressure distributions on the lee ($\theta = 0$) and weather ($\theta = \pi$) sides of the vertical cylinder as a function of depth for two different incident frequency combinations. We observe the dominant and slower attenuating second-order

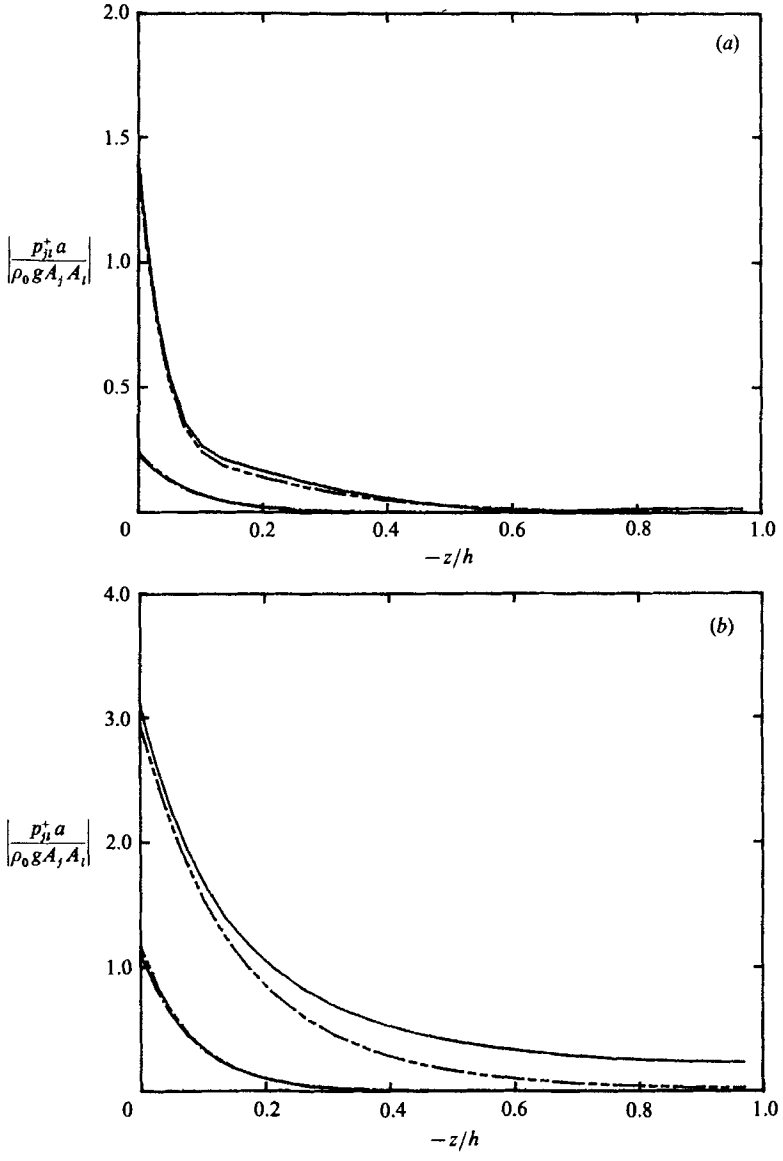

FIGURE 4. The second-order sum-frequency pressure QTF's on a uniform vertical cylinder ($h/a = 4$). The curves are for: $|p_{qjl}^{+}|$ for $\nu_j a, \nu_l a = 1, 2$ (—·—); 1.4, 1.6 (— — —); and $|p_{pjl}^{+}|$ for $\nu_j a, \nu_l a = 1$, 2 (— — — —); 1.4, 1.6 (——). (*a*) Lee side ($\theta = 0$); and (*b*) weather side ($\theta = \pi$).

potential pressure especially on the weather side (see (2.31)). This nonlinear potential pressure p_{p}^{+} appears to decrease only algebraically with depth in contrast to the expected exponential decay of the quadratic pressures p_{q}^{+} with wavenumber $(k_j + k_l)$. In (2.31), the far-field decay rate of ϕ_{p}^{+} with depth is angular dependent and given by the wavenumber $k_\theta = (k_j^2 + k_l^2 + 2k_j k_l \cos\theta)^{\frac{1}{2}}$, which has a minimum/maximum for $k_j = k_l$ and $\theta = \pi/0$ and increases with increasing $k_j - / + k_l$. One consequence is the behaviour of f_{p}^{+} in table 10, which has a maximum on the diagonal and decreases faster than f_{q}^{+} with increasing $\Delta\nu a$. Another effect is the increased moment arm associated with p_{p}^{+} which results in a significant contribution to the pitch moment

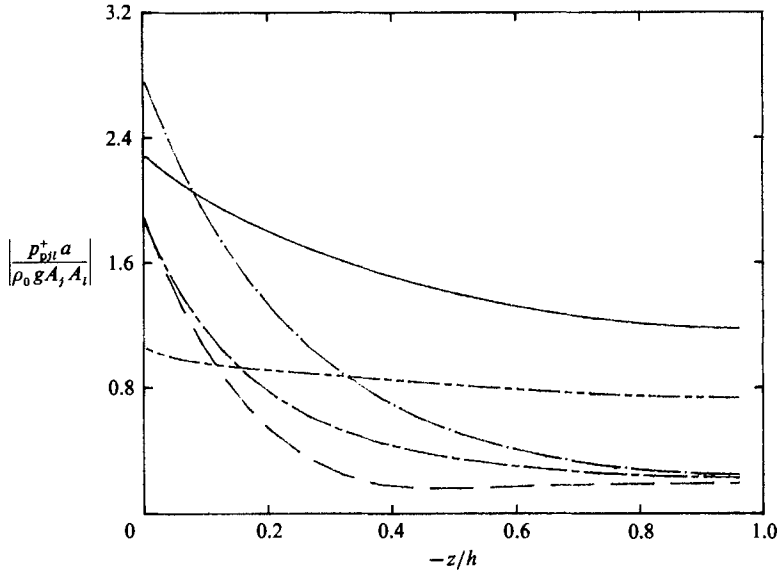

FIGURE 5. The sum-frequency second-order potential pressure QTF, $|p^+_{pjl}|$, on a uniform vertical cylinder ($h/a = 1$), for $(\nu_j a, \nu_l a) = (1, 2)$, and at angular positions: $\theta = 0$ (– – – – –), $\frac{1}{4}\pi$ (— · —), $\frac{1}{2}\pi$ (— — —), $\frac{3}{4}\pi$ (— — — —), and π (——).

QTF especially for deep draught bodies. It is noteworthy that when the free-surface component f^+_F is included in estimating the sum-frequency wave excitations on a tension-leg platform (Kim & Yue 1988), loadings several times greater than those obtained using only f^+_q, $\bar{\Delta}I^+_q$ are obtained. These predictions using the complete QTF are substantially supported by the large-scale tension-leg-platform experiments of Petrauskas & Liu (1987).

Figure 5 plots the second-order sum-frequency potential pressure QTF's, p^+_p, for the vertical cylinder of $h/a = 1$ as a function of depth at different angular positions for $(\nu_j a, \nu_l a) = (1, 2)$. In contrast to the difference-frequency problem (figure 2), variations in p^+_p for different θ are large owing to the dominant contribution from the angular-dependent free-surface pressures. As pointed out earlier, the decay rate at the waveward side is in general much slower than that of the leeward side. It is interesting that the minimum p^+_p may not occur at the bottom of the cylinder, for example, on the leeward ($\theta = 0$) side.

In figure 6, we present the second-order potential run-up QTF, η^+_p, and the quadratic contribution, η^+_q, on the $h/a = 1$ vertical cylinder for two different incident frequency combinations: $(\nu_j a, \nu_l a) = (1, 2)$ and $(1.4, 1.6)$. Unlike the difference-frequency problem (figure 3), both η^+_p and η^+_q are not sensitive to changes in $\Delta\nu a$. While the magnitude of η^+_q generally increases from the lee ($\theta = 0$) to weather side ($\theta = \pi$), that of η^+_p oscillates in θ, reaching peaks of comparable values $\theta = 0, \frac{1}{4}\pi$ and π.

We now turn to the hemisphere under sum-frequency excitation. Table 11 gives the horizontal and vertical sum-frequency force QTF's on a fixed hemisphere ($h/a = 3$). Again, the contributions associated with ϕ^+_I, f^+_I and f^+_{BI}, are negligible in the frequency range shown and are omitted. The horizontal force QTF components, f^+_q and f^+_p, are comparable in magnitude, while in the vertical direction, f^+_{pjl} is dominant over f^+_{qjl}. This is due to the appreciable second-order potential pressures on the

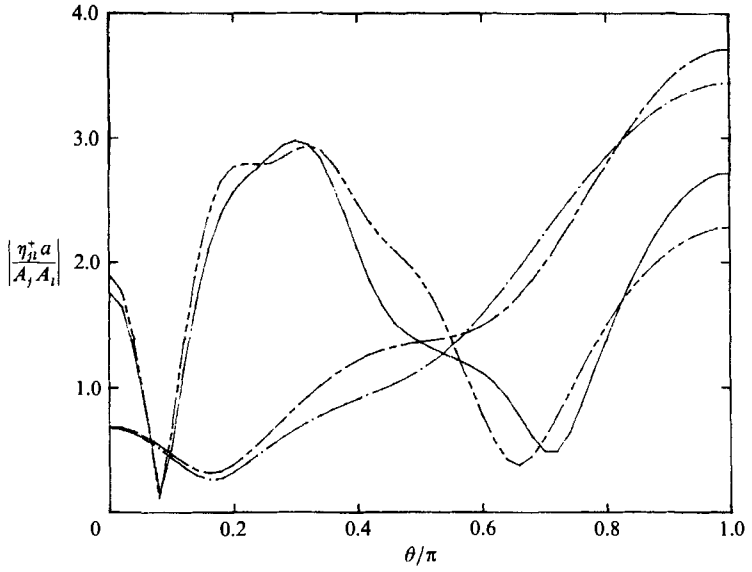

FIGURE 6. The second-order sum-frequency run-up QTF's, η^+_{qjl} and η^+_{pjl}, on a uniform vertical cylinder ($h/a = 1$). The curves are for: $|\eta^+_{qjl}|$ for $\nu_j a, \nu_l a = 1, 2$ (—·—); 1.4, 1.6 (– – –); and $|\eta^+_{pjl}|$ for $\nu_j a, \nu_l a = 1, 2$ (– – – –); 1.4, 1.6 (——).

bottom of the sphere. In both horizontal and vertical directions, f_q^+ and f_p^+ are generally out of phase, resulting in a smaller total QTF.

In figure 7, we plot the sum- and difference-frequency potential run-up QTF's, $\eta_p^{\pm}$, around a fixed sphere for two frequency combinations. Like the vertical cylinder case, η_p^+ is much greater than η_p^-. The general trends of η_p^- and η_p^+ are quite similar to those in figures 3 and 6, with η_p^+ having a more dominant peak on the weather side.

We finally give QTF results for the freely floating hemisphere and investigate the effect of first-order motions on the sum-frequency excitation (table 12). In contrast to the difference-frequency case (table 7), the body-surface forcing term due to first-order motions f_{BB}^+ contributes significantly in this case especially for vertical forces. Comparing to table 11, the increase of the quadratic term f_q^+ is quite noticeable especially near the heave natural frequency. This increase of f_q^+ and f_{BB}^+ near the heave natural frequency can barely be seen in the difference-frequency problem. In table 12, the three major contributions, f_q^+, f_{BB}^+, and f_p^+ (or f_F^+), are in general out of phase and hence the magnitude of the total QTF is much less than the sum of the individual components. With increasing sum frequency, the relative importance of f_F^+ increases over the other contributions, while f_{BB}^+ and f_q^+ continue to decrease. As a result, f_q^+ and f_{BB}^+ are the most important components in the low sum-frequency region, $(\nu_j + \nu_l)\, a < \sim 2.8$, whereas f_F^+ dominates the other contributions for $(\nu_j + \nu_l)\, a > \sim 2.8$.

6. Conclusion

The complete second-order sum- and difference-frequency diffraction problems for fixed or freely floating axisymmetric bodies in the presence of bichromatic incident waves are solved by the ring-source integral equation method. An important

$\nu_j a =$		0.8	1.0	1.2	1.4	1.6	1.8	2.0
$\nu_i a$	0.397	1.227	1.212	1.183	1.188	1.245	1.324	1.385
0.8	1.037	0.948	1.003	1.025	1.183	1.350	1.506	1.605
	0.642	0.835	0.783	0.751	0.749	0.741	0.717	0.676
	0.377	0.320	1.247	1.268	1.317	1.399	1.485	1.538
1.0	1.112	1.229	1.104	1.249	1.412	1.594	1.747	1.830
	0.737	0.914	0.730	0.704	0.692	0.681	0.655	0.610
	0.338	0.278	0.237	1.333	1.409	1.496	1.569	1.600
1.2	1.061	1.192	1.182	1.426	1.604	1.777	1.905	1.954
	0.725	0.918	0.948	0.663	0.642	0.628	0.603	0.560
	0.291	0.230	0.191	0.147	1.488	1.560	1.607	1.607
1.4	0.946	1.055	1.055	0.937	1.774	1.918	2.006	2.015
	0.656	0.827	0.865	0.790	0.614	0.600	0.579	0.541
	0.247	0.187	0.151	0.114	0.094	1.604	1.617	1.586
1.6	0.831	0.909	0.968	0.859	0.874	2.024	2.079	1.995
	0.584	0.722	0.819	0.745	0.781	0.592	0.585	0.518
	0.213	0.157	0.126	0.100	0.096	0.108	1.598	1.545
1.8	0.748	0.816	0.812	0.836	0.971	1.187	2.057	2.032
	0.534	0.660	0.687	0.736	0.877	1.083	0.563	0.570
	0.190	0.139	0.116	0.102	0.107	0.122	0.133	1.484
2.0	0.697	0.759	0.789	0.859	1.055	1.342	1.572	2.017
	0.507	0.620	0.673	0.758	0.951	1.225	1.444	0.606
$\nu_a =$	0.8	1.0	1.2	1.4	1.6	1.8	2.0	

TABLE 11. Magnitudes of the components of the second-order sum-frequency force QTF, $|f_{ji}^{+}/\rho_0 g a A_j A_i|$, on a fixed hemisphere ($h/a = 3$). The upper right triangular matrix is for the horizontal force, and the lower half the vertical force. Each element satisfies the symmetry relation, $f_{ji}^{+} = f_{ij}^{+}$. Computed values are for: first row, $|f_{qji}^{+}|$; second row, $|f_{pji}^{+}|$; and third row the complete QTF, $|f_{ji}^{+}|$.

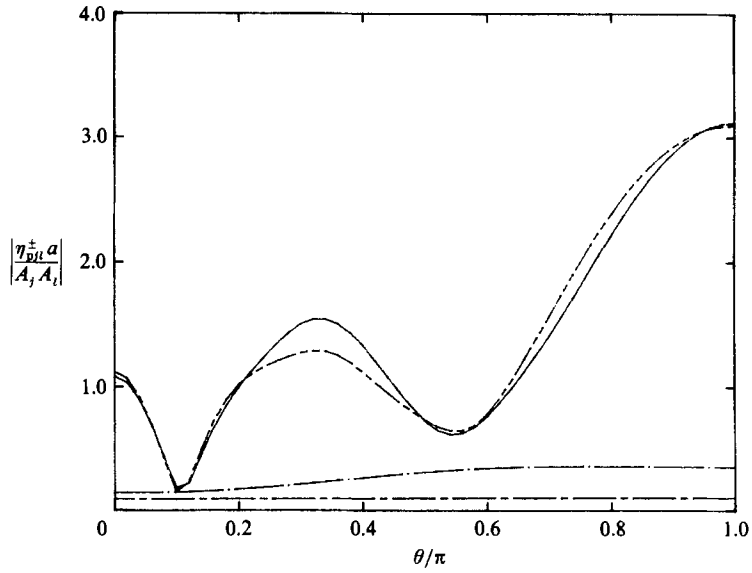

FIGURE 7. The sum- and difference-frequency second-order potential run-up QTF's, $\eta_{pji}^{\pm}$, on a fixed hemisphere on water depth $h = 3a$. The curves are for: $|\eta_{pji}^{-}|$ for $\nu_j a, \nu_i a = 1, 2$ (—·—); 1.4, 1.6 (– – –); and $|\eta_{pji}^{+}|$ for $\nu_j a, \nu_i a = 1, 2$ (– – – –); 1.4, 1.6 (——).

$\nu_j a =$		0.8	1.0	1.2	1.4	1.6	1.8	2.0
$\nu_i a$	1.485	1.244	1.878	1.697	1.293	1.149	1.091	1.040
0.8	1.641	0.681	0.861	0.617	0.379	0.326	0.314	0.305
	0.671	0.535	0.967	0.992	0.857	0.779	0.721	0.649
	0.131	0.541	0.756	0.673	0.486	0.407	0.358	0.328
	2.331	3.467	2.646	2.551	2.107	1.916	1.797	1.677
1.0	2.751	4.427	1.198	0.999	0.762	0.682	0.648	0.623
	0.894	0.984	1.573	1.767	1.568	1.459	1.357	1.226
	0.416	1.461	1.041	0.977	0.812	0.733	0.678	0.632
	1.885	2.702	2.085	2.871	2.548	2.373	2.263	2.151
1.2	2.461	3.826	3.219	1.031	0.829	0.727	0.675	0.642
	0.648	0.778	1.204	2.336	2.282	2.233	2.169	2.060
	0.628	1.877	2.338	1.067	0.948	0.879	0.822	0.761
	1.107	1.539	1.200	0.720	2.302	2.154	2.061	1.965
1.4	1.624	2.459	2.034	1.254	0.653	0.555	0.504	0.474
	0.327	0.565	1.134	1.142	2.293	2.266	2.216	2.117
	0.566	1.517	1.866	1.516	0.857	0.806	0.760	0.705
	0.712	0.962	0.771	0.496	0.378	2.010	1.916	1.823
1.6	1.177	1.747	1.483	0.897	0.638	0.458	0.409	0.368
	0.169	0.517	1.109	1.180	1.331	2.249	2.215	2.079
	0.525	1.280	1.632	1.372	1.383	0.778	0.759	0.694
	0.501	0.656	0.553	0.393	0.330	0.307	1.822	1.735
1.8	0.924	1.356	1.102	0.697	0.502	0.399	0.348	0.322
	0.104	0.522	1.022	1.204	1.456	1.696	2.169	2.141
	0.503	1.159	1.375	1.305	1.451	1.653	0.752	0.766
	0.375	0.473	0.431	0.340	0.306	0.295	0.284	1.665
2.0	0.763	1.103	0.901	0.575	0.419	0.338	0.288	0.291
	0.088	0.493	0.994	1.191	1.473	1.786	1.977	2.178
	0.479	1.051	1.278	1.254	1.450	1.734	1.918	0.829
$\nu_a =$	0.8	1.0	1.2	1.4	1.6	1.8	2.0	

TABLE 12. Magnitudes of the components of the sum-frequency force QTF, $|f_{ji}^{+}/\rho_0 g a A_j A_i|$, for a freely floating hemisphere ($h/a = 3$). The upper right triangular matrix is for the horizontal force, and the lower the vertical force. Each element satisfies the symmetry relation, $f_{ji}^{+} = f_{ij}^{+}$. Computed values are for: first row, $|f_{Qji}^{+}|$; second row, $|f_{BBji}^{+}|$; third row, $|f_{Iji}^{+} + f_{BIji}^{+} + f_{Fji}^{+}|$; and fourth row the total QTF, $|f_{ji}^{+}|$.

part of the solution is the efficient and accurate evaluation of the boundary forcing terms, particularly the integral on the entire free surface. An approach which treats the local-wave-free outer region analytically is developed and shown to be efficacious for both the sum- and difference-frequency problems. Although the second-order sum- and difference-frequency potentials are solved explicitly, the present method is comparable in computational effort (see §3) to the indirect approach which utilizes fictitious radiation potentials to obtain integrated quantities only. On the other hand, the availability of the second-order potential allows us to investigate and uncover many important local second-order phenomena in §5.

For illustration, extensive computations are performed for the sum- and difference-frequency diffraction by a bottom-mounted uniform vertical cylinder, and a fixed and a freely floating hemisphere. Systematic convergence tests are performed, and for the vertical cylinder, the results for the forces are checked against semi-analytic formulae developed in the Appendix.

From our numerical examples, several important features of the sum- and difference-frequency solutions can be observed:

Difference-frequency problem. Among the components of the total second-order difference-frequency force, the quadratic term, f_{q}^{-}, and second-order incident wave contributions, f_{I}^{-} and f_{BI}^{-}, are found to be the most important. The second-order incident potential, ϕ_{I}^{-}, attenuates slowly with depth especially for small frequency differences. As a result, f_{I}^{-} and f_{BI}^{-} are particularly important when the draught of the body is large or when major portions of the body are deeply submerged. In this case, widely used approximation such as those of Newman (1974), Marthinsen (1983), and Standing & Dacunha (1982), may substantially *underestimate* the slowly varying forces and moments. On the other hand, Pinkster's (1980) or QIB approximations are found to be useful for a broad range of incident frequency combinations. The second-order potential pressures and run-up are primarily associated with the second-order incident wave and are relatively constant around the body, especially when the two primary incident frequencies are close.

Sum-frequency problem. In contrast to the difference-frequency problem, the second-order diffraction potential ϕ_{D}^{+}, or more precisely the locked wave potential ϕ_{p}^{+} associated with the free-surface forcing, plays a dominant role. As a result, existing approximations which all exclude this contribution are inadequate and may substantially *underestimate* the sum-frequency wave loads. The contributions associated with ϕ_{I}^{+} in this case are negligible except for the long wave (or shallow water) regime. Unlike the difference-frequency problem, the body-boundary forcing contribution from first-order motions, f_{BB}^{+}, has an important effect on the sum-frequency forces on an oscillating body. As in the monochromatic case, the second-order diffraction potential ϕ_{D}^{+} attenuates slowly with depth on the waveward side. Interestingly, the penetration is deeper for smaller frequency differences of the incident waves. As a result, the pitch moments on a deep-draught body can be greatly amplified owing to p_{p}^{+}, particularly when the centre of rotation is close to the free surface. The sum-frequency second-order potential pressures and run-up have large variations around the body owing to significant contributions from the angular dependent free-surface forcing pressures.

The present theory and numerical results for bichromatic waves can be directly used for estimating the statistics of sum- and difference-frequency wave excitations and responses in general Gaussian irregular seas. In this case, the random sea surface can be expressed as a sum of N regular wave components:

$$\zeta(t) = \mathrm{Re} \sum_{j=1}^{N} A_j \mathrm{e}^{-\mathrm{i}\omega_j t} \quad (A_j = a_j \mathrm{e}^{\mathrm{i}\epsilon_j}), \tag{6.1}$$

where a_j and ϵ_j are the amplitude and phase of the jth component wave, and the random phase ϵ_j is uniformly distributed in 0 and 2π. The component amplitude a_j is given by $a_j = (2S(\omega_j)\,\Delta\omega)^{\frac{1}{2}}$, where $S(\omega)$ is the one-sided wave amplitude spectrum. Given the input wave spectrum and the second-order force QTF's, the time series of the sum/difference frequency excitations can be directly calculated from

$$F_{\mathrm{ex}}^{(2)}(t) = \mathrm{Re} \sum_{j=1}^{N} \sum_{l=1}^{N} [A_j A_l^{*} f_{jl}^{-} \mathrm{e}^{-\mathrm{i}(\omega_j - \omega_l)t} + A_j A_l f_{jl}^{+} \mathrm{e}^{-\mathrm{i}(\omega_j + \omega_l)t}], \tag{6.2}$$

where the sum- and difference-frequency force QTF's satisfy the symmetry relations, $f_{jl}^{-} = f_{lj}^{-*}$ and $f_{jl}^{+} = f_{lj}^{+}$. Equation (6.2) is equivalent to the two-term Volterra series expression (Neal 1974) after performing a double Fourier transform. Upon deriving

the autocorrelation function of $F_{ex}^{(2)}(t)$ in continuous form, the one-sided spectra of sum- and difference-frequency forces can be obtained:

$$S_F(\omega^-) = 8\int_0^\infty S(\mu)\,S(\mu+\omega^-)\,|f^-(\mu,\mu+\omega^-)|^2\,\mathrm{d}\mu, \tag{6.3}$$

$$S_F(\omega^+) = 8\int_0^{\frac{1}{2}\omega^+} S(\tfrac{1}{2}\omega^+ + \mu)\,S(\tfrac{1}{2}\omega^+ - \mu)\,|f^+(\tfrac{1}{2}\omega^+ + \mu, \tfrac{1}{2}\omega^+ - \mu)|^2\,\mathrm{d}\mu. \tag{6.4}$$

A theory for the probability distribution of $F_{ex}^{(2)}(t)$, which is non-Gaussian, is available, and is detailed for example in Neal (1974).

This research was supported by the US National Science Foundation and the Office of Naval Research. DKPY also acknowledges partial support from the Henry L. Doherty Chair. Some of the computations were conducted on the Cray X-MP/48 at the Pittsburgh Supercomputer Center and on the Cray-2S at Cray Research.

Appendix. Semi-analytic solutions for the second-order sum- and difference-frequency forces on a bottom-mounted uniform vertical circular cylinder

For a single regular wave, the closed-form expression for the second-order double-frequency horizontal force was obtained by Molin & Marion (1986) and Eatock Taylor & Hung (1987), and extended to include the overturning moment also in KY-I. Here, we generalize this problem to bichromatic incident waves and sum- and difference-frequency forces. For a uniform vertical circular cylinder of radius a in water depth h, the explicit expression for the first-order total potential for wave component j is

$$\phi_j^{(1)} = \frac{-\mathrm{i}gA_j}{\omega_j}\frac{\cosh k_j(z+h)}{\cosh k_j h}\sum_{n=0}^{\infty}\epsilon_n\,\mathrm{i}^n\left[J_n(k_j\rho) - \frac{J_n'(k_j a)}{H_n'(k_j a)}H_n(k_j\rho)\right]\cos n\theta, \tag{A 1}$$

where a prime represents differentiation with respect to the argument. Substituting (A 1) into (4.19) and (4.20) and performing the integration in θ, we obtain the quadratic components of the second-order forces, $f_{qjl}^{\pm}$, as follows:

$$\frac{f_{qjl}^+}{\rho_0 g a A_j A_l} = \frac{2\mathrm{i}}{\pi(k_j a)(k_l a)}\sum_{n=0}^{\infty}(-1)^n\,\Omega_{njl}^+\left[1 + \frac{(k_j H)(k_l h)}{\omega_j\omega_l h/g}\frac{(I^- + I^+ n(n+1)/(k_j a)(k_l a))}{\cosh k_j h\cosh k_l h}\right], \tag{A 2}$$

$$\frac{f_{qjl}^-}{\rho_0 g a A_j A_l^*} = \frac{-2\mathrm{i}}{\pi(k_j a)(k_l a)}\sum_{n=0}^{\infty}\Omega_{njl}^-\left[1 - \frac{(k_j h)(k_l h)}{\omega_j\omega_l h/g}\frac{(I^- + I^+ n(n+1)/(k_j a)(k_l a))}{\cosh k_j h\cosh k_l h}\right], \tag{A 3}$$

where

$$\Omega_{njl}^+ = \frac{1}{H_{n+1}'(k_j a)\,H_n'(k_l a)} + \frac{1}{H_n'(k_j a)\,H_{n+1}'(k_l a)}, \tag{A 4}$$

$$\Omega_{njl}^- = \frac{1}{H_{n+1}'(k_j a)\,H_n'^*(k_l a)} - \frac{1}{H_n'(k_j a)\,H_{n+1}'^*(k_l a)}, \tag{A 5}$$

$$I^\pm = \frac{1}{2}\left[\frac{\sinh k^+ h}{k^+ h} \pm \frac{\sinh k^- h}{k^- h}\right]. \tag{A 6}$$

The second-order Froude–Krylov excitation QTF's, $f^{\pm}_{1jl}$, can be obtained from the first integral of (4.21), which yields

$$f^{\pm}_{1jl} = \pi a \rho_0 \omega^{\pm} \begin{bmatrix} (\gamma^{+}_{jl} + \gamma^{+}_{lj}) \\ (\gamma^{-}_{jl} + \gamma^{-*}_{lj}) \end{bmatrix} \frac{\tanh k^{\pm} h}{k^{\pm}} J_1(k^{\pm} a), \tag{A 7}$$

where $\gamma^{\pm}_{jl}$ are given in (2.6) and (2.7).

The second-order diffraction potential contributions can be evaluated from (4.23) in terms of the sum- and difference-frequency assisting radiation potentials for horizontal translation, $\Psi^{\pm}_x$, which have the explicit expressions

$$\Psi^{\pm}_x = \cos\theta \left[B^{\pm}_0 \frac{\cosh k^{\pm}_2 (z+h)}{k^{\pm}_2} \frac{H_1(k^{\pm}_2 \rho)}{H'_1(k^{\pm}_2 a)} + \sum_{m=1}^{\infty} B^{\pm}_m \frac{\cos \kappa^{\pm}_{2m}(z+h)}{\kappa^{\pm}_{2m}} \frac{K_1(\kappa^{\pm}_{2m}\rho)}{K'_1(\kappa^{\pm}_{2m} a)} \right], \tag{A 8}$$

where K is the second-kind modified Bessel function. The coefficients $B^{\pm}$ in (A 8) are given by

$$B^{\pm}_m = \frac{4 \sinh k^{\pm}_{2m} h}{2k^{\pm}_{2m} h + \sinh 2k^{\pm}_{2m} h} \quad (m = 0, 1, 2, \ldots), \tag{A 9}$$

where $k_{20} = k_2$, $k_{2m} = \mathrm{i}\kappa_{2m}$, and κ_{2m} are associated with the evanescent modes and are given by the real roots of the dispersion relation

$$\omega^{\pm 2} = -\kappa^{\pm}_{2m} g \tan \kappa^{\pm}_{2m} h, \quad (m - \tfrac{1}{2})\pi \leqslant \kappa^{\pm}_{2m} h \leqslant m\pi. \tag{A 10}$$

Upon integrating the first right-hand side integral of (4.23), the body forcing contribution is obtained in explicit forms:

$$f^{\pm}_{\mathrm{B}jl} = -\pi \rho_0 a \omega^{\pm} \begin{bmatrix} (\gamma^{+}_{jl} + \gamma^{+}_{lj}) \\ (\gamma^{-}_{jl} + \gamma^{-*}_{lj}) \end{bmatrix} \frac{k^{\pm} h J'_1(k^{\pm} a)}{\cosh k^{\pm} h} \left[B^{\pm}_0 \Pi^{\pm}_0 \frac{H_1(k^{\pm}_2 a)}{k^{\pm}_2 H'_1(k^{\pm}_2 a)} + \sum_{m=1}^{\infty} B^{\pm}_m \Pi^{\pm}_m \frac{K_1(\kappa^{\pm}_{2m} a)}{\kappa^{\pm}_{2m} K'_1(\kappa^{\pm}_{2m} a)} \right]. \tag{A 11}$$

where

$$\Pi^{\pm}_m = \frac{1}{2} \left[\frac{\sinh (k^{\pm} + k^{\pm}_{2m}) h}{k^{\pm} + k^{\pm}_{2m}} + \frac{\sinh (k^{\pm} - k^{\pm}_{2m}) h}{k^{\pm} - k^{\pm}_{2m}} \right], \quad m = 0, 1, 2, \ldots. \tag{A 12}$$

From (3.4*b*) and (A 1), the sum- and difference-frequency free-surface forcing for $n = 1$ are given by

$$q^{\pm}_{1jl} = \frac{2g^2 A_j A_l k_j^2}{\omega_j} \sum_{m=0}^{\infty} \begin{bmatrix} (-1)^m \\ 1 \end{bmatrix} \left[\left(\Lambda_{jl} + \frac{k_l}{k_j} \frac{m(m+1)}{(k_j \rho)(k_l \rho)} \right) \Gamma^{\pm}_m + \frac{k_l}{k_j} \hat{\Gamma}^{\pm}_m \right], \tag{A 13}$$

where Λ_{jl} is given in (3.16) and

$$\Gamma^{+}_m = Z^j_{m+1} Z^l_m + Z^j_m Z^l_{m+1} - J^j_{m+1} J^l_m - J^j_m J^l_{m+1}, \tag{A 14}$$

$$\hat{\Gamma}^{+}_m = Z'^j_{m+1} Z'^l_m + Z'^j_m Z'^l_{m+1} - J'^j_{m+1} J'^l_m - J'^j_m J'^l_{m+1}, \tag{A 15}$$

$$Z^j_m = J_m(k_j \rho) - \frac{J'_m(k_j a)}{H'_m(k_j a)} H_m(k_j \rho). \tag{A 16}$$

The corresponding difference-frequency terms in (A 14) and (A 15) can be obtained by taking the complex conjugate of the terms containing superscript l. Finally the

free-surface forcing contributions in (4.23) are given by the infinite line integral whose behaviour is very similar to (3.12):

$$f_{Fjl}^{\pm} = \frac{i\pi\rho_0\omega^{\pm}}{g}\int_a^{\infty} d\rho\,\rho Q_1^{\pm}[\Psi_x^{\pm}]_{z=0,\theta=0} \tag{A 17}$$

REFERENCES

Benschop, A., Hermans, A. J. & Huijsmans, R. H. M. 1987 Second order diffraction forces on a ship in irregular waves. *Appl. Ocean Res.* **9**, 96–104.

Bowers, E. C. 1976 Long period oscillations of moored ships subject to short wave seas. *Trans. R. Inst. Naval Archit.* **118**, 181–191.

De Boom, W. C., Pinkster, J. A. & Tan, S. G. 1983 Motion and tether force prediction for a deep water Tension Leg Platform. *Proc. Offshore Technology Conf.*, no. 4487. OTC, Houston.

Eatock Taylor, R. & Hung, S. M. 1987 Second order diffraction forces on a vertical cylinder in regular waves. *Appl. Ocean. Res.* **9**, 19–30.

Eatock Taylor, R., Hung, S. M. & Mitchell, K. L. 1988 Advances in the prediction of low frequency drift behavior. In *Proc. Behavior of Offshore Structures*, pp. 651–666. BOSS, Norway.

Herfjord, K. & Nielsen, F. G. 1986 Nonlinear wave forces on a fixed vertical cylinder due to the sum frequency of waves in irregular seas. *Appl. Ocean Res.* **8**, 8–21.

Hulme, A. 1982 The wave forces acting on a floating hemisphere undergoing forced periodic oscillations. *J. Fluid Mech.* **121**, 443–463.

John, F. 1950 On the motion of floating bodies; 2. *Commun. Pure Appl. Math.* **3**, 45–101.

Kagemoto, H. & Yue, D. K. P. 1986 Interactions among multiple three-dimensional bodies in water waves: an exact algebraic method. *J. Fluid Mech.* **166**, 189–209.

Kim, M. H. & Yue, D. K. P. 1988 The nonlinear sum-frequency wave excitation and response of a tension-leg platform. *5th Intl Conf. Behavior Offshore Structures.* BOSS, Norway.

Kim, M. H. & Yue, D. K. P. 1989 The complete second-order diffraction solution for an axisymmetric body. Part 1. Monochromatic incident waves. *J. Fluid Mech.* **200**, 235–264 (referred to as KY-I).

Lighthill, M. J. 1979 Waves and hydrodynamic loading. *Proc. 2nd Intl Conf. Behavior Offshore Structures*, pp. 1–40. BOSS, London.

Loken, A. E. 1986 Three dimensional second order hydrodynamic effects on ocean structures in waves. *Rep.* UR-86-54. University of Tronheim, Dept of Marine Technology.

Marthinsen, T. 1983 Calculation of slowly varying drift forces. *Appl. Ocean Res.* **5**, 141–144.

Matsui, T. 1988 Computation of slowly varying second order hydrodynamic forces on floating structures in irregular waves. In *Proc. Offshore Mechanics & Arctic Engineering*, vol. 1, pp. 117–124. OMAE, Houston.

Molin, B. 1979 Second order diffraction loads upon three dimensional bodies. *Appl. Ocean Res.* **1**, 197–202.

Molin, B. 1983 On second order motion and vertical drift forces for three dimensional bodies in regular waves. *Intl Workshop Ship & Platform Motions, Berkeley*, pp. 344–362.

Molin, B. & Marion, A. 1986 Second order loads and motions for floating bodies in regular waves. *Proc. Offshore Mechanics & Arctic Engineering*, vol. 1, pp. 353–360. OMAE, Tokyo.

Neal, E. 1974 Second order hydrodynamic forces due to stochastic excitation. *Proc. 10th Symp. on Naval Hydrodynamics.*

Newman, J. N. 1974 Second order slowly varying forces on vessels in irregular waves. *Symp. on Dynamics of Marine Vehicles and Structures in Waves, London.*

Ogilvie, T. F. 1983 Second order hydrodynamic effects on ocean platforms. *Intl Workshop Ship & Platform Motion, Berkeley*, pp. 205–265.

Petrauskas, C. & Liu, S. V. 1987 Springing force response of a tension leg platform. *Proc. Offshore Technology Conf.*, no. 5458. OTC, Houston.

Pinkster, J. A. 1980 Low frequency second order wave exciting forces on floating structures. *NSMB Rep.* 650.

STANDING, R. G. & DACUNHA, N. M. C. 1982 Slowly varying and mean second-order wave forces on ships and offshore structures. *Proc. 14th Symp. on Naval Hydrodynamics, Ann Arbor.*

URSELL, F. 1953 The long wave paradox in the theory of gravity waves. *Proc. Camb. Phil. Soc.* **49**, 685–694.

WANG, P. F. 1987 The radiation condition and numerical aspects of second order surface wave radiation and diffraction. Ph.D. thesis, MIT. Dept of Ocean Engineering.

WATSON, G. N. 1952 *A Treatise on the Theory of Bessel Functions.* Cambridge University Press.